

Cross-section measurements for electron-impact ionization of atoms

Robert S. Freund, Robert C. Wetzel, Randy J. Shul, and Todd R. Hayes
 AT&T Bell Laboratories, Murray Hill, New Jersey 07974

(Received 6 October 1989)

Absolute electron-impact cross sections have been measured from 0 to 200 eV for single ionization of 16 atoms (Mg, Fe, Cu, Ag, Al, Si, Ge, Sn, Pb, P, As, Sb, Bi, S, Se, and Te) with an estimated accuracy of $\pm 10\%$. Combined with our recent measurements of He, Ne, Ar, Kr, Xe, F, Cl, Br, I, Ga, and In [Wetzel *et al.*, Phys. Rev. A **35**, 559 (1987); Hayes *et al.*, *ibid.* **35**, 578 (1987); Shul, Wetzel, and Freund, *ibid.* **39**, 5588 (1989)], a set of 27 atomic single-ionization cross sections has now been measured with the same apparatus. In addition, cross sections are reported for double ionization of ten atoms and triple ionization of eight atoms. The measurements are made by crossing an electron beam with a 3-keV beam of neutral atoms, prepared by charge-transfer neutralization of a mass-selected ion beam. The critical measurement of absolute neutral beam flux is made with a calibrated pyroelectric crystal. The magnitudes of the single-ionization-peak cross sections decrease monotonically across rows of the periodic table from group IIIA (Al,Ga,In) to group VIIIA (Ar,Kr,Xe), varying much more than predicted by various empirical formulas and classical and quantum-mechanical theories.

I. INTRODUCTION

Electron-impact ionization is one of the most fundamental collision processes in atomic and molecular physics. It sustains gas discharges and plasmas, leads to most of the chemistry in radiation effects, plays a major role in planetary upper atmospheres, and is the basis for much of mass spectrometry. Because of their basic and practical importance, cross sections for electron-impact ionization have been measured since the earliest days of atomic collision physics.¹⁻³ Several reviews of previous measurements have been published.⁴⁻⁹ In addition, much work has recently been done on ionization of ions to higher charge states.^{7,10}

Nevertheless, measurements of absolute cross sections for electron-impact ionization as a function of electron energy have been reported for only 33 neutral atoms, about $\frac{1}{3}$ of the atoms in the Periodic Table (Fig. 1). Most of these have been of gases (the rare gases), or of solids that vaporize easily (the alkali metals). Measurements of atoms that vaporize only at high temperatures or are extremely reactive have been prevented by the difficulty of measuring absolute pressure or beam flux, or by the inability to obtain (and verify) pure beams. Of the 33 atomic cross sections that have been measured before, the most accurately known are those of He (Refs. 11-13) and Ar,¹²⁻¹⁵ for which several independent workers agree to within $\pm 7\%$. Recent measurements, which are probably of comparable accuracy, are for Ne,^{11,13} Kr,^{11,13} H,¹⁶ C,¹² N,¹² and O.^{12,17} The alkali atoms [Li,¹⁸⁻²¹ Na,^{18-20,22} K,^{18-20,22,23} Rb,^{19,20,22,24} Cs (Refs. 19, 20, 22, 25, and 26)], alkaline-earth atoms [Mg,²⁷⁻³¹ Ca,³¹⁻³³ Sr,³¹⁻³³ Ba (Refs. 31-34)], and Pb (Refs. 34-36) have been measured several times, with agreement in the range of 10-30%. For several other atoms [Cu,^{35,37,38} Ag,^{35,39} Al,⁴⁰⁻⁴² Ga,^{40,41,43} In,^{40,41,43} Tl (Refs. 32, 40, 41)], two or three measurements exist, but they differ by 50% or more, and

sometimes disagree in shape from threshold to 200 eV. For other atoms [S,⁴⁴ Yb,⁴⁵ U,⁴⁶ Hg,⁴ Au (Ref. 38)], only a single measurement exists.

This paper reports ionization cross section measurements of 16 atoms, ten of which have not been measured before (Fig. 1). These new measurements, when combined with our recent measurements of the rare gas,¹³ halogen,⁴⁷ gallium,⁴⁸ and indium atoms,⁴⁸ make a set of 27 cross sections measured with the same apparatus. In addition, the combination of this work and our previous measurements^{13,47} provides 22 measurements of double ionization and 15 of triple ionization. Since no previous workers have used the same apparatus to measure ionization cross sections of more than five different atoms, it is now possible for the first time to identify a number of systematic trends.

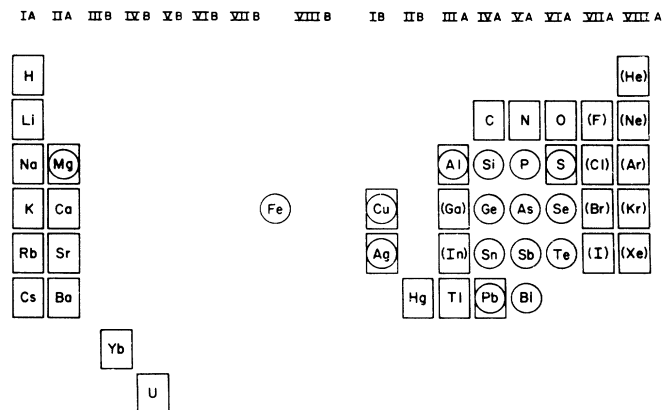


FIG. 1. Atoms for which electron-impact ionization cross sections have been measured. Squares represent atoms for which previous measurements exist, circles represent atoms reported in this work, and parentheses represent atoms previously measured by this laboratory.

II. EXPERIMENT

The present work uses the crossed-electron-beam-fast-atom-beam method, in which a beam of neutral atoms is prepared by charge-transfer neutralization of a mass-selected ion beam and is then ionized by a well-characterized electron beam. The apparatus (Fig. 2) has been described in detail before.^{13,49} Briefly, a 3-keV ion beam is extracted from a dc discharge and velocity selected with a Wien filter to isolate one mass. The ions then pass through a region of low-pressure gas ($\sim 10^{-4}$ Torr), where neutral atoms are formed by charge transfer. The remaining ions are then deflected out of the beam. A region of high electric field (over 5000 V/cm) then ionizes and removes most Rydberg atoms (which also form by charge transfer). The atom beam then crosses a 0–200-eV electron beam. The overlap of these two beams is measured. The product ions are focused at the entrance of a hemispherical energy analyzer, which serves to separate ions of different mass to charge ratios, and after leaving the analyzer are pulse counted using a channel electron multiplier (CEM). The absolute neutral beam flux is measured with a calibrated pyroelectric detector. The cross section is given by¹³

$$\sigma = I_i v / I_e R F, \quad (1)$$

where v is the velocity of the atomic beam, I_e is the electron current, R is the flux of neutral atoms, F is the overlap between the electron and atomic beams, and I_i is the current of ions to the detector, is $1.602 \times 10^{-19} C_{\text{corr}} / K \epsilon$, where C_{corr} is the measured count rate corrected for dead time, K is the fraction of ions transmitted to the CEM face ($K = 1$), and ϵ is the counting efficiency of the CEM.

A. Beam sources

Ion beams are generated from a hot-tungsten-filament dc discharge, using a Colutron ion source⁵⁰ oriented with its axis horizontal. Most of our early work used discharges in permanent gases to form ions, but some

ions were formed from a rare-gas discharge with the standard Colutron solid source,⁴⁸ a stainless steel sample holder coaxial with the helical filament. In this work we use a more convenient approach, with chemistry similar to that of previous work.⁵¹ A small sample containing the element of interest is placed directly inside the cylindrical Pyrex insulator which supports the anode and a discharge is run through CCl_4 . The ion formation mechanism is probably the reaction of Cl atoms with the sample to form volatile chlorides, followed by their dissociation in the discharge to form atoms and ions. Diatomic and triatomic chloride ions were often seen in the mass spectra of these sources. Ions of more volatile materials, such as phosphorus, could be formed with rare-gas discharges rather than with CCl_4 . For species which rapidly etched the pinhole in the tantalum anode, we spot-welded a platinum foil with a matching pinhole on the inside of the anode. These sources generally gave usable beams for 4–12 h; the limit to usable life was usually instabilities, rather than loss of intensity. The source materials and typical beam intensities are given in Table I.

Ion beams from the source generally contain other ions in addition to the atomic ion of interest. These include atomic Cl^+ and diatomic or polyatomic chlorides. There was often a small contribution at mass 28, most likely N_2 from a small leak in the inlet line or as an impurity in the source gas. Possibly it included CO from outgassing of the hot source. These impurities were easy to remove with the Wien filter, except for measurements on Si (mass 28). In this case, mass scans with the hemispherical energy analyzer were used to look for fragment ions. The absence of N^+ or C^+ and O^+ set an upper limit of about 5% to the impurity level of N_2 or CO in the Si beam.

B. Charge transfer

The gas most commonly used for charge-transfer neutralization was triethylamine (TEA). It was chosen because its ionization potential (IP) (about 8.1 eV vertical^{52,53} and 7.2 eV adiabatic⁵²) is close to the IP of many

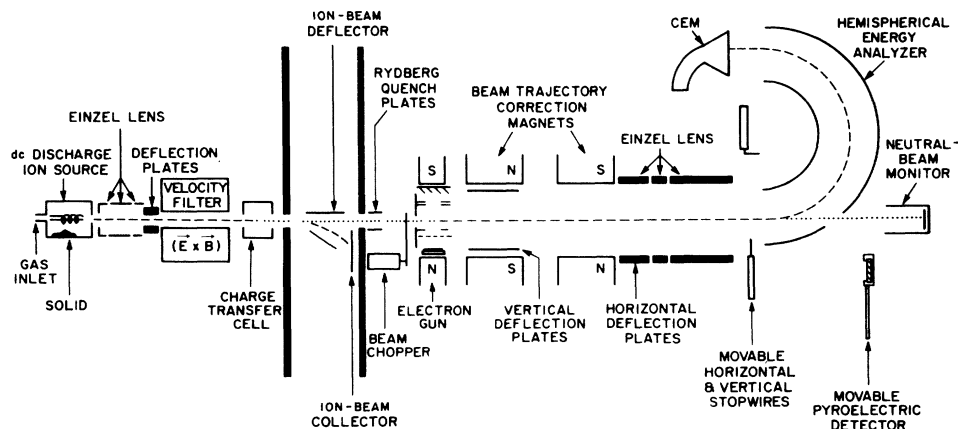


FIG. 2. Apparatus.

of the atoms studied here (Table I). This near resonance should enhance the charge-transfer cross section. Charge transfer of TEA with atoms with higher IP's can take place from electrons in inner orbitals. Charge-transfer gases with higher ionization potentials were used to neutralize atoms with higher ionization potentials, as listed in Table I. In the cases of Al, Ga, In, and Ag, the gas used is far from resonant with the ground-state ion. For these atoms, charge transfer is most likely to occur with ions in metastable electronic states, for which the resonance condition more nearly applies.⁴⁸

In addition to producing atoms in the ground electronic state, charge-transfer neutralization also produces atoms in Rydberg states. Those with principal quantum number n above 19 are removed by electric field ionization. Those with n below 8 have lifetimes shorter than the time of flight to the electron beam. Those with n between 8 and 19 survive to the electron beam where they are ionized by electron collisions. Since these ions follow the same trajectory as ions from ground-state atoms, their counts at the detector are indistinguishable from

ground-state ionization other than by their extremely low threshold energies and the shapes of their ionization cross sections. Their contribution is subtracted from the measured data according to the procedure described previously.¹³

C. Experimental improvements

Since the early measurements of ionization cross sections from this laboratory,^{13,47,49,54-56} several technique changes have been made which improve accuracy and reproducibility.

The original method of measuring the electron-beam profile used a set of ten narrow slots in the anode with a separate collector behind each slot. That method provided a continuous measurement of the electron-beam profile which proved itself unnecessary; the electron-beam profile remained constant throughout measurements and from day to day. The original method of measuring the neutral-beam profile was to scan a knife edge across the beam and take the derivative of the

TABLE I. Source conditions, charge-transfer gases, and beam intensities. In this and subsequent tables, atoms are listed in order of increasing atomic number.

Atom	E_{IP} (eV)	Source		Charge-transfer gas	I_{ion} (μA)	I_{neut} (NA)	Signal (10^3 counts/sec)	Background (10^3 counts/sec)	signal/background
		Solid	Gas						
Mg	7.61	Mg	CCl ₄	TEA ^a	1.5	3	2.5	3.8	0.7
Al	5.96	Al	CCl ₄	CP ^b	1.0	1	3.5	42.0	0.1
Si	8.15	Si	SiF ₄	TEA	0.4	2	6.2	11.0	0.6
P	10.9	GaP	CCl ₄	EY ^c	0.3	0.7	3.1	11.7	0.3
P	10.9	GaP	CCl ₄	TEA	0.3	1.5	1.6	13.7	0.1
S	10.3		CS ₂	CP	0.3	2.3	6.8	37.0	0.2
Cl	13.0		CCl ₄	EY	0.4	1.5	2.6	23.0	0.1
Ar	15.7		Ar	Ar	1.0	1.5	7.0	4.0	1.8
Fe	7.83	FeCl ₃	Kr	TEA	0.1	1	7.2	30.2	0.2
Cu	7.68	Cu	CCl ₄	TEA	0.5	0.7	4.0	47.0	0.1
Ga	5.97	GaP	Ar	Xe	0.65	1	2.0	3.6	0.6
Ga	5.97	Ga	CCl ₄	TEA	0.45	1	1.2	10.2	0.1
Ge	8.09	Ge	CCl ₄	TEA	0.15	1	16.3	6.1	2.7
As	10.5	GaAs	Ar	CP	0.25	0.6	22.0	19.6	1.1
As	10.5	As	Ar	CP	0.15	1.5	22.0	22.0	1.0
Se	9.70	Se	CCl ₄	CP	0.35	1.2	10.4	10.3	1.0
Br	11.8		CF ₂ Br ₂	ET ^d					
Kr	13.9		Kr	Kr	1.0	1.3	12.0	10.0	1.2
Ag	7.54	Ag	CCl ₄	ET	1.5	0.5	9.1	6.2	1.5
In	5.76	In	CCl ₄	TEA	0.7	1	33.0	14.7	2.2
In	5.76	InP	Ne	TEA	0.9	0.5	16.9	7.0	2.4
Sn	7.30	Sn	CCl ₄	TEA	1.0	2.1	35.5	8.8	4.0
Sb	8.5	Sb	CCl ₄	TEA	0.35	1.5	26.0	29.0	0.9
Te	8.96	Te	CCl ₄	BU ^e	0.8	2.5	45.0	5.0	9.0
I	10.6	NaI	Ne/Kr	ET					
Xe	12.1		Xe	Xe	1.0	1.5	30.0	7.5	4.0
Pb	7.38	Pb	CCl ₄	TEA	0.7	0.8	21.0	2.2	9.6
Bi	8.0	Bi	CCl ₄	TEA	1.0	1	48.0	3.3	1.5

^aTEA is triethylamine.

^bCP is cyclopropane.

^cEY is ethylene.

^dET is ethane.

^eBU is 1,3-butadiene.

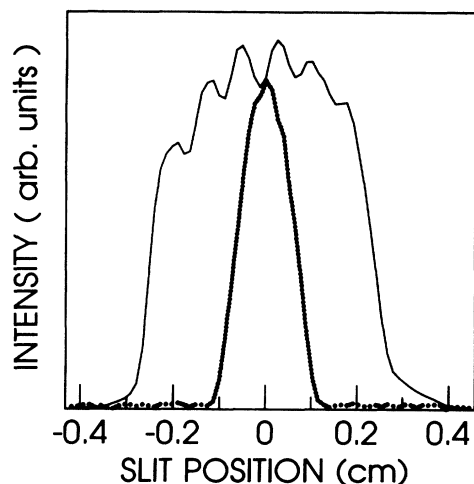


FIG. 3. Overlap of neutral-beam and electron-beam profiles, measured by scanning a 0.010-in. slit across the beams and measuring the transmitted electron current (solid line) and neutral-beam flux (dotted line). The shadow of the grid wires is clearly visible on the electron-beam profile.

transmitted signal. The result was an excessively noisy measurement, which also was difficult to align with the electron beam. We therefore changed to the conventional method for measuring overlap,⁵⁷ a 0.010-in. slit scanned across both beams simultaneously. An example of one measurement is shown in Fig. 3. Such a measurement was made before and after every absolute cross-section measurement. The width of the neutral beam reflects the 0.093-in. square collimating aperture in front of the electron beam. Shadows of the grid wires are clearly seen in the electron-beam profile. The spacing of the dips matches the 0.08-cm spacing of the grid wires. The overlap factors measured over more than a year are nearly constant, falling in the small range of 2.00–2.27 cm^{-1} .

Reduction of the chamber base pressure lowered the flux of ions formed by collisional ionization, improving the signal-to-noise ratio. Collisional ionization occurs when electrons are stripped from fast neutral atoms colliding with the background gas. These ions have nearly the same velocities and trajectories as ions formed by electron impact. To keep them from overloading the CEM in pulse counting mode, the neutral-beam intensity had to be limited. This background was directly proportional to the pressure along the beam path. The working pressure in the main vacuum chamber was improved in two ways. Originally, this chamber was pumped by an oil diffusion pump without liquid nitrogen, giving a base pressure of 2×10^{-8} Torr. Replacing this pump with an 8-in. cryopump lowered the base pressure by more than an order of magnitude to 1×10^{-9} Torr. The second improvement was to move the charge-transfer cell from the middle chamber to the source chamber, in effect adding a stage of differential pumping.

The most important improvement in the method of measurement came from the calibration of the pyroelectric crystal response to the neutral beam. The principal cause of unstable response in the earlier work was the use

of a relatively intense ion beam (10^{-7} A) to calibrate the pyroelectric detector before each cross-section measurement. This ion beam charged trace insulating films on the surface, leading to variable extraneous currents in phase with the chopped ion and neutral beams. When only neutral beams were allowed to strike the pyroelectric detector, the response was usually found to be constant for a few weeks.

The solution, therefore, has been to use the well-known Ar and Kr ionization cross sections to calibrate the response of the pyroelectric. Previous values of the Ar and Kr cross sections^{11,13–15,58–64} are summarized in Table II. There is excellent agreement for four independent absolute measurements of $\sigma(\text{Ar})$ and two of $\sigma(\text{Kr})$. In addition there is agreement within 6% of ten independent measurements of the ratio of $\sigma(\text{Kr})$ to $\sigma(\text{Ar})$ at 70 eV. Our present measurement of the $\sigma(\text{Kr})$ to $\sigma(\text{Ar})$ ratio is 1.53 ± 0.07 , in agreement with the average of the previous values to well within the uncertainties. We therefore believe that $\sigma(\text{Ar})$ or $\sigma(\text{Kr})$ can be used equally well as reference cross sections. Since our Kr signal-to-noise ratio was somewhat better than that for Ar, we used as reference the Kr single-ionization cross-section value at 70 eV of 3.72 \AA^2 (Table III). One or two full days of calibrations were run every time the pyroelectric crystal was changed or the chamber was vented to atmosphere (twice during the year of these measurements). Ar or Kr cross sections were then remeasured every week or two. All of these measurements reproduced the value used for calibration within $\pm 4\%$, demonstrating the stability of the detector (and the remainder of the measurement procedure). As a further check on our use of the Ar and Kr cross sections, we show in Fig. 4 the difference between our measured single-ionization cross sections and the accepted measurements of Rapp and Englander-Golden (REG).¹¹ Since they measured total ionization cross sections, we have subtracted from their data the contributions of double and triple ionization.¹³ The agreement is from +4% to –2% over the energy range 0–200 eV, except for a few points near thresholds where a small error of either our energy scale or REG's leads to a larger percentage difference.

The remaining improvements also involved measurement of the neutral-beam flux. Previously, the lock-in amplifier was zeroed by closing an electropneumatic valve between chambers. This induced electrical transients, changed the pressure in the main chamber, and may have obscured the small background to the pyroelectric detector from sources such as infrared radiation from the hot ion source. The solution has been to first measure the neutral-beam signal and then detune the Wien filter to a setting between resolved mass peaks and subtract this base line. With the added stability of this method, it became possible to measure weaker neutral beams and discover another source of error, a small zero offset in the lock-in which led to variations of the calculated cross sections as a function of neutral-beam flux for the weakest beams. Incorporating an additive constant to the flux in the analysis gave zero offsets mostly in the range –1 to –4 μV . When these offsets could be measured they were used in deriving the cross section, and when they could

TABLE II. Absolute total electron-impact ionization cross sections for Ar and Kr, and ratios of the Kr to Ar total ionization cross sections at 70 eV. Literature values of cross sections reported at 75 eV have been corrected to 70 eV by multiplying them by 1.008, based on the cross-section shapes reported in Ref. 11. Ratios of single ionization at 70 eV have been corrected to ratios of total ionization by multiplying by 1.029, based on double-ionization cross sections at 70 eV of 0.13 \AA^2 for Ar and 0.24 \AA^2 for Kr as given in Ref. 13. The 1.53 ± 0.07 ratio measured in the present work is based on seven measurements of the Ar cross section with a standard deviation of 3.1% and ten measurements of the Kr cross section with a standard deviation of 3.1%. All measurements were made over a one week period.

Reference	Year	Absolute total cross sections		Ratio
		$\sigma(\text{Ar})$	$\sigma(\text{Kr})$	$\sigma(\text{Kr})/\sigma(\text{Ar})$
58 ^a	1957			1.48
59	1960			1.39 \pm 0.10
60	1963			1.56 \pm 0.15
11	1965	2.77 \pm 0.19	4.21 \pm 0.29	1.52 \pm 0.07
62 ^a	1966			1.48
61	1969			1.46
14	1973	3.00 \pm 0.12		
15	1974	2.87 \pm 0.14		
63 ^a	1975			1.52 \pm 0.06
64 ^a	1983			1.46
13 ^b	1987	2.93 \pm 0.49	4.19 \pm 0.57	1.43 \pm 0.30
This work	1989			1.53 \pm 0.07
Average		2.90 \pm 0.14	4.20 \pm 0.28	1.48 \pm 0.05 ^c

^aOriginally reported at 75 eV.

^bThe uncertainties are large because they represent independent absolute measurements; no measurement was made of the rare-gas cross sections relative to each other.

^cAverage and standard deviation of 10 ratio measurements.

TABLE III. Measured absolute cross sections for single ionization (\AA^2) at 70 eV, peak energies, and peak cross sections.

Atom	Cross section \pm Standard deviation (70 eV)	Standard deviation (%)	Number of values	E_{IP} (eV)	Peak energy (E_p)	E_p/E_{IP}	Cross section at peak (\AA^2)
Mg	3.07 \pm 0.10	3	6	7.61	20	2.6	5.30
Al	7.82 \pm 0.38	5	8	5.96	24	4.0	9.90
Si	5.79 \pm 0.23	4	20	8.15	27	3.3	6.69
P	4.91 \pm 0.14	3	12	9.1 ^a	36	3.3	5.26
S	4.41 \pm 0.20	5	7	10.3	36	3.5	4.50
Cl	3.51 \pm 0.12	3	3	13.0	60	4.6	3.49
Ar	2.64 ^b			15.7	50	3.2	2.62
Fe	4.38 \pm 0.17	4	9	7.83	29	3.7	5.34
Cu	3.47 \pm 0.22	6	10	7.68	27	3.5	4.09
Ga	8.26 \pm 0.34	4	9	5.97	29	4.9	9.19
Ge	6.64 \pm 0.15	2	8	8.09	32	4.0	7.46
As	5.69 \pm 0.15	3	8	8.5 ^a	40	3.8	6.12
Se	5.73 \pm 0.35	6	5	9.70	45	4.6	5.90
Kr	3.72 ^b			13.9	70	5.0	3.72
Ag	5.24 \pm 0.20	4	12	7.54	45	6.0	5.47
In	9.91 \pm 0.56	6	11	5.76	27	4.7	12.17
Sn	8.42 \pm 0.16	2	7	7.30	30	4.1	9.77
Sb	7.40 \pm 0.26	4	7	7.5 ^a	32	3.8	8.32
Te	7.92 \pm 0.10	1	6	8.96	32	3.6	8.27
Xe	5.35 \pm 0.18	3	6	12.1	40	3.3	4.80
Pb	7.27 \pm 0.24	3	8	7.38	32	4.3	8.32
Bi	8.01 \pm 0.08	1	6	5.63 ^a	36	4.5	8.75

^aIP of 2D state.

^bReference value, calculated from the total ionization cross sections of Table II minus twice the double-ionization cross section from Ref. 13.

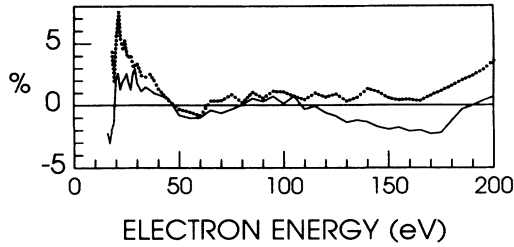


FIG. 4. Shape comparisons between the present measurements of $\sigma(\text{Ar})$ (· · ·) and $\sigma(\text{Kr})$ (—) and those of Rapp and Englander-Golden (Ref. 11). Data are displayed as $[\sigma(\text{REG})-\sigma(\text{AT\&T})]/\sigma(\text{REG})$.

not be measured, an approximate correction of $-1.4 \mu\text{V}$ was used. Whenever strong enough neutral beams could be obtained ($\geq 30 \mu\text{V}$ referred to the input of the lock-in) data taken with the weaker beams were discarded.

A final improvement in the neutral-beam flux measurement was the method used to determine the duty cycle of the chopped neutral beam (the neutral beam was chopped only for its flux measurement, not for cross-section measurements). The old method¹³ monitored the neutral beam with the secondary emission detector and measured the secondary electron current with an electrometer. The long electrometer time constant (~ 10 sec) averaged the chopped current. The duty cycle was the ratio of this average to the continuous current with the chopper turned off. The low currents and long time constant limited the accuracy of this measurement. The improved method monitors the neutral beam by ionizing it and counting ions with the CEM. The ratios of counts from chopped and unchopped beams gave the duty cycle directly, with an accuracy of about $\pm 2\%$.

With these improvements, Eq. (1) can be reduced, in a way similar to that used in Ref. 13, to the following expression for the cross section (in cm^2) depending only on measured quantities:

$$\sigma = 3.5 \times 10^{-32} C_{\text{corr}} E^{3/2} D \phi / I_e \epsilon M^{1/2} F N, \quad (2)$$

where E is the translational energy of the atomic beam (always 3000 eV in this work), D is the duty cycle of the chopped neutral beam (about 0.5), ϵ is the counting efficiency of the CEM, M is mass in atomic units, F is the overlap between electron and atomic beams, and N is the output of the lock-in amplifier in μV . ϕ includes the sensitivity of the pyroelectric detector and several other instrumental factors; it is determined from Eq. (2) using measurements of $\sigma(\text{Ar})$ and $\sigma(\text{Kr})$ and their known cross sections.

D. Error estimate

The systematic uncertainty of absolute cross-section measurements made with this apparatus and reported in Ref. 13 was $\pm 12\%$. Within the subsequent technique improvements, the accuracy has improved considerably. Many important sources of systematic error in the absolute measurements (Table I of Ref. 13) are greatly reduced or vanish by using the Ar and Kr cross sections as

references.

In our previous work,¹³ the uncertainty in the electron current I_e was dominated by systematic corrections for reflected ($\pm 5\%$) and secondary ($\pm 3\%$) electrons. These uncertainties are now identical for measurement of the unknown atom and the reference atom, so they cancel.

The previous electron-beam profile measurement ($\pm 5\%$) made at ten discrete positions has now been replaced by the overlap F measured with a scanned slit, where F is defined as⁴

$$F = \frac{\int j_n(z) j_e(z) dz}{\int j_n(z) dz \int j_e(z) dz}, \quad (3)$$

with the z direction perpendicular to both the electron and neutral beams. F was measured as part of every cross-section measurement. If there is any systematic error in this value, it will tend to be the same for the unknown atom and the rare-gas reference atom, and so cancel.

Systematic uncertainties in the ion count rate are dominated by the detector efficiency ϵ . The systematic uncertainty in ϵ ($\epsilon = \epsilon_1 \epsilon_2 \epsilon_3$) was previously estimated to be $\pm 8\%$, where ϵ_1 is the probability that an incident ion ejects at least one electron upon impact with the CEM, ϵ_2 is the probability that a secondary electron formed at the CEM cone is collected by the CEM channel, and ϵ_3 is the probability that an electron which reaches the CEM channel is eventually counted by the electronics. ϵ_2 and ϵ_3 should be the same for all atoms, and so contribute nothing to the systematic uncertainty. ϵ_1 was previously estimated as 0.95 ± 0.05 , with a maximum possible value of 1.00. We now float the CEM so the output end is at -2 kV and the input is approximately -5 kV. Thus ions now strike the entrance cone with energies 2 kV greater than in the previous experiments, so we expect ϵ_1 to be even closer to unity. Its value may vary for different atoms, however, and so it remains a source of systematic uncertainty. We therefore estimate the systematic uncertainty of the difference between an unknown atom and a reference atom to be $\pm 4\%$, a value slightly smaller than the previously estimated 5% systematic uncertainty for the absolute value of ϵ_1 .

There are several possible atom-dependent errors in the measurement of the neutral-beam flux. Particles sputtered from the pyroelectric detector can carry energy away. We estimated¹³ that a maximum of 5% of the incident energy would be lost, so the difference between the energy sputtered by the unknown and reference atoms must be smaller, estimated here as 2%. Similarly, loss of secondary electrons from the pyroelectric detector could lead to atom-dependent spurious currents indistinguishable from signal. These secondary electrons are repelled back to the detector by a -150-V bias on the hemispheres during neutral-beam flux measurements, so we estimate this error as only 1%. Two other potential sources of error come from the ion source. Impurity neutrals may be present in the beam due to charge-transfer neutralization of ions before the mass filter. Since these neutrals form before the end of the source ion optics, they are not focused and so should be weak. Similarly,

infrared radiation from the hot ion source could affect the pyroelectric detector. Both of these contributions are corrected for, in part, by the background subtraction made by setting the Wien filter between mass peaks. We estimate the residual uncertainty as 1%. Finally, there is the nonlinearity of the lock-in amplifier for very small signals. Although corrections were made for this effect, the uncertainty could be 3%. When these uncertainties are combined in quadrature, the systematic uncertainty of a neutral-beam flux measurement is 4%.

The systematic uncertainty of the pyroelectric calibration constant is dominated by the uncertainties of the Ar and Kr cross sections used as reference, $\pm 5\%$ and $\pm 6.6\%$, respectively, but since there are other systematic and random errors in converting the rare-gas cross section to a value of ϕ , we take the accuracy of ϕ to be $\pm 7\%$. Systematic uncertainties in the remaining factors E , D , M , and N should be small, and since they should be the same for the unknown and the reference atoms, they cancel. Thus the systematic uncertainty is dominated by ϵ with an uncertainty of $\pm 4\%$, R with an uncertainty of 4%, and ϕ with an uncertainty of $\pm 7\%$, which when combined in quadrature give a systematic uncertainty of $\pm 9\%$.

Random uncertainties tend to be small. For example, the overlap F for all the measurements in this work fell between 2.00 and 2.27 cm^{-1} with a standard deviation (random) of $\pm 2\%$. The random uncertainties of other measured quantities are determined primarily by fluctuations in meter readings. Thus we estimate the random uncertainties to be 2% for D , I_e , F , and N , and essentially 0% for E and M . Combined in quadrature these values give a $\pm 4\%$ random uncertainty. This estimate is corroborated by the scatter in replicate measurements of the cross sections for each atom as given in Table III, where the standard deviations range from 1% to 6%.

Combining systematic and random uncertainties gives $\pm 10\%$ as the overall one-standard-deviation uncertainty for the absolute cross-section values. The uncertainty of the atomic cross sections relative to each other should be smaller, however, since they all use $\sigma(\text{Kr})$ as a reference; thus the 7% absolute uncertainty of $\sigma(\text{Kr})$ does not enter into the relative uncertainty. The resulting systematic uncertainty of the cross sections for one atom relative to another is $\pm 5\%$, and the combined systematic and random uncertainties is approximately $\pm 7\%$.

III. RESULTS

A. Absolute cross sections

Measurements of absolute cross sections for single ionization at 70 eV are given in Table III. Between 5 and 20 measurements were made for each atom, usually on two or more days, with standard deviations ranging from 1% to 6%. As a check on the absolute accuracy, Cl was remeasured and found to be $3.51 \pm 0.12 \text{ \AA}^2$ at 70 eV, only 1% larger than the value of 3.47 from Ref. 47.

B. Ratios

Ratios of double-to-single and triple-to-single ionization cross sections are given in Table IV. At least two

TABLE IV. Measured double-to-single ionization ratios at 100 eV, and triple-to-single ionization ratios at 150 eV, \pm Standard deviation (number of measurements). n/a indicates data which were too weak to be measured.

Atom	2+ / +	3+ / +
Mg	n/a	n/a
Al	n/a	n/a
Si	$0.0523 \pm 0.0020(4)$	n/a
P	$0.0518 \pm 0.0057(12)^a$	n/a
S	$0.0510 \pm 0.0052(8)$	n/a
Cl	0.067 (1)	n/a
Fe	$0.0604 \pm 0.0062(6)$	n/a
Cu	$0.0553 \pm 0.0004(3)$	n/a
Ga	$0.065 \pm 0.0006(3)$	0.0061(1)
Ge	$0.0816 \pm 0.0021(3)$	$0.0052 \pm 0.0006(3)$
As	$0.0683 \pm 0.0012(4)$	$0.0102 \pm 0.0003(4)$
Se	$0.0697 \pm 0.0003(2)$	$0.0085 \pm 0.0016(2)$
Ag	$0.1027 \pm 0.0022(4)$	$0.0188 \pm 0.0009(4)$
In	$0.130 \pm 0.0078(2)$	$0.0240 \pm 0.0029(2)$
Sn	$0.1546 \pm 0.0021(3)$	$0.0268 \pm 0.0015(3)$
Sb	$0.117 \pm 0.0047(5)$	$0.0392 \pm 0.0017(5)$
Te	$0.0983 \pm 0.0008(4)$	$0.0326 \pm 0.0013(4)$
Pb	$0.2293 \pm 0.0053(3)$	$0.0339 \pm 0.0016(3)$
Bi	$0.161 \pm 0.0010(3)$	$0.0423 \pm 0.0008(3)$

^aMeasured at 100 eV: six with TEA, six with ethylene.

measurements were made of each ratio, with standard deviations better than 11% for the double-to-single ratios and 12% for the triple-to-single ratios. Occasional measurements at other electron energies of absolute cross sections and multiple-to-single ionization ratios confirm the 0–200-eV shapes, to within the experimental uncertainties.

C. Shapes

The cross-section shapes for formation of single, double, and triple ions were measured for electron energies from threshold to 200 eV at 1-eV intervals. Several independent runs were corrected for measured variations in the electron current and then added together to improve the signal-to-noise ratio. Shape corrections, less than 5%, were also made below 50 eV and above 150 eV according to Eq. (15) in Ref. 13. The absolute measurements and ratios were then used to normalize the relative 0–200-eV measurements. Cross sections from 0–200 eV for single, double, and triple ionization of the 18 atoms measured in this work are shown in Fig. 5 and are tabulated in Table V. For some of the atoms, the double- and triple-ionization data were not measured since the signals were very weak. The shape of each cross section has been measured at least twice and the results averaged. Sources lasted generally about 8 h, so individual runs were limited to 2–4 h, to permit more than one type of measurement to be made with the same source on the same day. Above 30 eV, values at several adjacent energies are averaged. The 0–200-eV shapes for single ionization were normal-

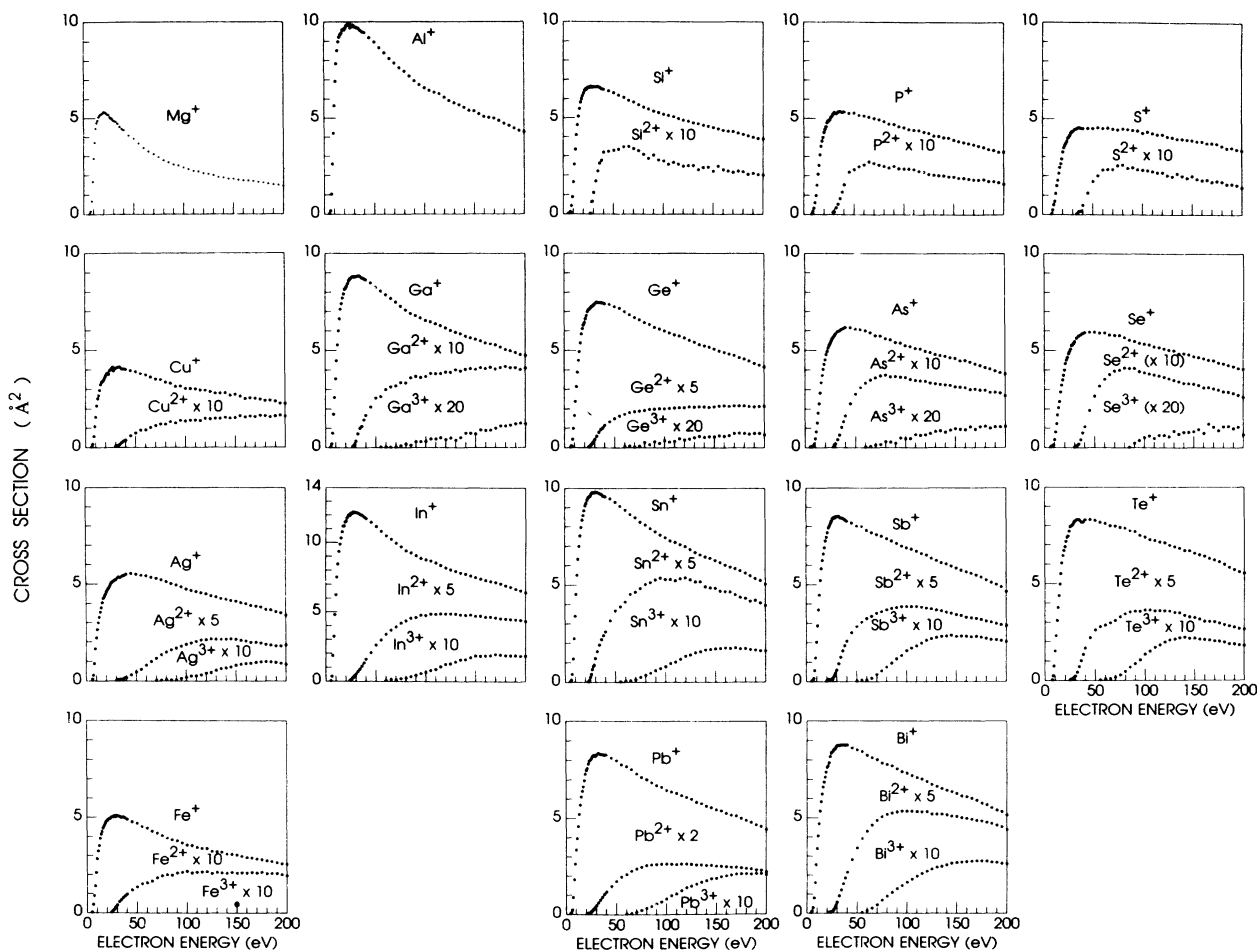


FIG. 5. 0–200-eV cross sections for 18 atoms.

ized to the absolute cross section at 70 eV; the shapes for double and triple ionization were then normalized to the single-ionization cross section using the measured ratios.

D. Threshold measurements

Careful threshold measurements of the single-ionization cross sections (Fig. 6) serve to characterize the states present in the atomic beam. The energy scales were calibrated with Eq. (1) of Ref. 49, which accounts for space charge and contact potentials. Curvature is about 0.5 eV for the sharpest thresholds, consistent with the energy spread of the electron beam and the small ground-state fine structure. For five of the atoms Mg, Ag, Al, Ga, and In and the previously measured halogen and rare-gas atoms, the first excited state energy is so high that only the ground state can be expected to form by charge transfer. The data show thresholds at the ionization potentials, indicated by vertical lines. As expected for an atom with an isolated ground state, Ga gave identical thresholds and cross sections, within experimental uncertainty, for two different charge-transfer gases. The remaining atoms have low-lying excited states, so we must determine if any of their excited states are popu-

lated in the atomic beam. The occurrence of a threshold below the IP is evidence that an excited state is populated, since an excited state could reach the ground-state ion with less energy than the IP. The Si, Ge, S, and Se atoms have thresholds which are at the IP, showing that only the ground state is present in the neutral beam.

The remaining thresholds show that excited states are present in those beams. The excited states of Sn, Pb, and Te appear to be fine-structure components of the ground electronic state. Thus their ionization cross sections should be nearly identical to those of the ground fine-structure component. For Fe, Cu, and the group VA atoms P, As, Sb, and Bi, excited electronic states appear to be populated. The threshold for Fe is about 3 eV below the IP. We identified approximately 30 electronic states of Fe within 3 eV of the ground state which could be ionized with less than 7.83 eV. Thus the Fe cross section presented here is of questionable significance since it reflects an average over many unspecified states. Analysis of the original Cu data shows that about 30% of the Cu beam is in the 2D excited state, with fine-structure components at 1.39 and 1.64 eV. All four atoms in group VA (P, As, Sb, and Bi) are primarily in their first excited states (2D), lying 1–2 eV above the ground state. This is

TABLE V. Measured cross sections (\AA^2) for electron impact single, double, and triple ionization from 0 to 200 eV.

Electron Energy (eV)	Mg ⁺	Al ⁺	Si ⁺	Si ²⁺	P ⁺	P ²⁺	S ⁺	S ²⁺	Cl ²⁺	Fe ⁺	Fe ²⁺	Cu ⁺	Cu ²⁺	Ga ⁺	Ga ²⁺	Ga ³⁺
5		0.00								0.00				0.00		
6	0.00	0.14	0.01							0.42		0.00		0.17		
7	0.12	0.99	0.07							0.89		0.13		0.72		
8	0.65	2.54	0.39		0.00					1.44		0.53		1.73		
9	1.64	4.15	0.86		0.13		0.00			2.18		1.03		2.61		
10	2.85	5.61	1.63		0.30		0.21			2.95		1.52		3.59		
11	3.68	6.88	2.56		0.57		0.47			3.38		2.11		4.55		
12	4.43	7.79	3.34		0.93		0.65			3.69		2.47		5.36		
13	4.72	8.47	4.12		1.45		1.06			4.09		2.64		6.10		
14	4.85	8.93	4.65		2.01		1.45			4.32		2.90		6.74		
15	5.03	9.18	5.12		2.47		1.72			4.47		3.19		7.25		
16	5.12	9.31	5.52		3.01		2.09			4.67		3.32		7.54		
17	5.17	9.37	5.85		3.46		2.39			4.77		3.35		7.85		
18	5.20	9.54	6.05		3.71		2.59			4.90		3.42		8.06		
19	5.23	9.57	6.20		3.91		2.84			5.03		3.55		8.30		
20	5.30	9.56	6.34		4.16		3.21			5.07		3.67		8.36		
21	5.28	9.64	6.48		4.33		3.43			5.14		3.76		8.48		
22	5.26	9.76	6.56		4.47		3.56			5.17		3.78		8.66		
23	5.18	9.78	6.53		4.67		3.66			5.18		3.72		8.76		
24	5.17	9.90	6.63		4.78		3.77			5.26		3.92		8.89		
25	5.15	9.87	6.64		4.78		3.95			5.28	0.00	3.95		8.91		
26	5.02	9.65	6.64		4.85		4.00			5.28	0.01	4.02		8.93		
27	4.97	9.71	6.69	0.00	4.98		4.08			5.32	0.01	4.09		8.94	0.00	
28	4.97	9.79	6.65	0.06	5.03		4.20			5.26	0.03	3.90		8.98	0.01	
29	4.89	9.78	6.66	0.06	5.15		4.26			5.34	0.03	4.01		9.00	0.02	
30	4.83	9.71	6.67	0.11	5.20	0.01	4.29			5.32	0.04	4.02		9.04	0.03	
32	4.79	9.67	6.66	0.17	5.16	0.03	4.39			5.30	0.06	4.08	0.00	9.14	0.07	
34	4.68	9.63	6.69	0.22	5.24	0.05	4.43	0.00		5.22	0.07	4.09	0.01	9.19	0.10	
36	4.52	9.52	6.63	0.26	5.26	0.08	4.50	0.01		5.26	0.08	4.00	0.03	9.13	0.12	
38	4.41	9.44	6.56	0.28	5.21	0.11	4.46	0.01	0.00	5.20	0.09	4.00	0.03	9.15	0.15	
40	4.34	9.41	6.54	0.32	5.24	0.15	4.44	0.04	0.02	5.13	0.10	3.98	0.03	9.14	0.18	
45	4.05	9.14	6.46	0.32	5.17	0.21	4.44	0.11	0.04	4.99	0.12	3.91	0.06	9.06	0.23	
50	3.88	8.91	6.36	0.33	5.18	0.23	4.44	0.17	0.07	4.91	0.14	3.84	0.07	8.92	0.28	
55	3.63	8.61	6.23	0.33	5.07	0.24	4.49	0.20	0.12	4.73	0.16	3.76	0.08	8.74	0.29	
60	3.39	8.34	6.12	0.35	5.04	0.25	4.45	0.23	0.12	4.64	0.16	3.68	0.09	8.62	0.33	
65	3.21	8.05	5.96	0.35	4.98	0.27	4.47	0.23	0.15	4.49	0.17	3.58	0.10	8.45	0.34	
70	3.07	7.82	5.87	0.34	4.91	0.26	4.41	0.23	0.17	4.38	0.19	3.47	0.11	8.26	0.35	0.000
75	2.90	7.57	5.72	0.33	4.85	0.25	4.38	0.25	0.17	4.24	0.20	3.44	0.12	8.08	0.37	0.003
80	2.74	7.40	5.61	0.31	4.75	0.24	4.42	0.25	0.17	4.12	0.21	3.31	0.11	7.90	0.37	0.008
85	2.64	7.14	5.50	0.29	4.62	0.24	4.40	0.24	0.18	4.01	0.20	3.26	0.13	7.77	0.40	0.005
90	2.53	6.90	5.39	0.31	4.60	0.24	4.36	0.24	0.17	3.95	0.22	3.09	0.12	7.68	0.40	0.015
95	2.48	6.70	5.31	0.28	4.49	0.23	4.33	0.23	0.18	3.84	0.22	3.11	0.13	7.56	0.40	0.015
100	2.37	6.53	5.24	0.27	4.43	0.23	4.21	0.23	0.18	3.72	0.22	2.99	0.13	7.44	0.40	0.015
105	2.28	6.40	5.17	0.26	4.34	0.23	4.27	0.22	0.18	3.70	0.22	2.98	0.13	7.42	0.42	0.023
110	2.19	6.30	5.09	0.27	4.29	0.23	4.19	0.22	0.18	3.59	0.22	2.96	0.14	7.32	0.42	0.023
115	2.16	6.22	5.00	0.26	4.28	0.22	4.13	0.21	0.18	3.55	0.22	2.89	0.13	7.21	0.42	0.026
120	2.07	6.04	4.90	0.25	4.19	0.21	4.13	0.21	0.17	3.53	0.22	2.90	0.15	7.09	0.43	0.021
125	2.03	5.87	4.86	0.25	4.13	0.20	4.01	0.20	0.18	3.39	0.21	2.82	0.14	6.97	0.42	0.025
130	1.97	5.75	4.77	0.25	4.00	0.20	3.98	0.19	0.18	3.36	0.22	2.74	0.15	6.89	0.44	0.019
135	1.87	5.66	4.71	0.23	3.97	0.20	3.90	0.21	0.17	3.34	0.22	2.74	0.15	6.80	0.43	0.026
140	1.84	5.51	4.64	0.24	3.91	0.19	3.89	0.19	0.17	3.22	0.22	2.75	0.15	6.74	0.44	0.039
145	1.78	5.35	4.57	0.24	3.89	0.19	3.86	0.18	0.17	3.21	0.22	2.63	0.15	6.67	0.45	0.039
150	1.76	5.32	4.50	0.22	3.78	0.19	3.83	0.20	0.17	3.17	0.22	2.68	0.15	6.57	0.44	0.037
155	1.72	5.17	4.44	0.24	3.73	0.18	3.77	0.18	0.17	3.11	0.22	2.58	0.16	6.54	0.45	0.048
160	1.69	5.03	4.36	0.23	3.66	0.18	3.76	0.17	0.16	3.04	0.22	2.46	0.15	6.41	0.45	0.046
165	1.68	4.98	4.32	0.22	3.61	0.18	3.68	0.18	0.16	3.02	0.22	2.50	0.16	6.39	0.45	0.048
170	1.65	4.94	4.29	0.21	3.55	0.17	3.68	0.16	0.16	2.95	0.22	2.47	0.15	6.33	0.44	0.053
175	1.61	4.82	4.22	0.22	3.48	0.17	3.64	0.17	0.15	2.92	0.22	2.43	0.16	6.24	0.45	0.059
180	1.58	4.67	4.14	0.22	3.41	0.18	3.52	0.17	0.15	2.86	0.21	2.37	0.16	6.14	0.46	0.060
185	1.53	4.56	4.07	0.20	3.32	0.17	3.41	0.15	0.15	2.81	0.22	2.37	0.15	6.06	0.45	0.062
190	1.49	4.42	4.00	0.21	3.27	0.17	3.43	0.15	0.15	2.75	0.21	2.33	0.16	5.98	0.45	0.065
195	1.46	4.30	3.93	0.20	3.18	0.16	3.35	0.15	0.14	2.67	0.21	2.22	0.16	5.87	0.44	0.068
200	1.41	4.22	3.90	0.20	3.18	0.15	3.30	0.14	0.14	2.66	0.20	2.21	0.16	5.84	0.45	0.066

TABLE V. (Continued.)

	Ge ⁺	Ge ²⁺	Ge ³⁺	As ⁺	As ²⁺	As ³⁺	Se ⁺	Se ²⁺	Se ³⁺	Ag ⁺	Ag ²⁺	Ag ³⁺	In ⁺	In ²⁺	In ³⁺
5				0.00						0.00			0.00		
6	0.00			0.02						0.05			0.31		
7	0.07			0.03			0.00			0.26			1.78		
8	0.40			0.05			0.04			0.83			3.17		
9	0.95			0.16			0.11			1.59			4.74		
10	1.62			0.42			0.38			2.14			6.19		
11	2.34			0.78			0.77			2.57			7.45		
12	3.10			1.23			1.19			2.92			8.39		
13	3.85			1.74			1.65			3.20			9.29		
14	4.46			2.23			2.03			3.47			9.81		
15	4.90			2.78			2.35			3.70			10.26		
16	5.34			3.31			2.83			3.97			10.72		
17	5.80			3.68			3.19			4.18			11.13		
18	6.08			3.99			3.46			4.28			11.14		
19	6.27			4.24			3.69			4.39			11.43		
20	6.40			4.48			3.96			4.50			11.48		
21	6.59			4.74			4.29			4.61			11.72		
22	6.75			4.91			4.48			4.70			11.87		
23	6.96			5.09			4.61			4.78			11.95		
24	7.07	0.00		5.21			4.80			4.88			11.91	0.00	
25	7.09	0.01		5.30			4.91			5.00			12.07	0.01	
26	7.15	0.02		5.42			5.03			5.08			12.05	0.03	
27	7.22	0.03		5.54			5.22			5.10			12.17	0.04	
28	7.24	0.04		5.61	0.00		5.25			5.03			12.13	0.06	
29	7.29	0.06		5.68	0.01		5.31			5.05			12.14	0.07	
30	7.36	0.08		5.78	0.02		5.41			5.16			12.12	0.09	
32	7.46	0.11		5.90	0.04		5.59	0.00		5.27			12.07	0.13	
34	7.42	0.15		5.94	0.06		5.69	0.02		5.26			11.98	0.17	
36	7.42	0.18		6.02	0.10		5.75	0.04		5.33	0.01		11.91	0.21	
38	7.41	0.20		6.07	0.13		5.82	0.07		5.37	0.02		11.79	0.25	
40	7.37	0.22		6.12	0.16		5.87	0.10		5.43	0.03		11.68	0.31	
45	7.34	0.26		6.11	0.22		5.90	0.19		5.47	0.06		11.42	0.40	
50	7.22	0.29		6.04	0.27		5.90	0.26		5.42	0.08		11.10	0.51	
55	7.13	0.32		6.01	0.31		5.85	0.31		5.37	0.11		10.76	0.58	
60	6.96	0.34	0.001	5.95	0.33		5.86	0.35		5.35	0.15		10.44	0.67	0.00
65	6.80	0.36	0.003	5.85	0.34	0.001	5.75	0.37		5.26	0.19		10.19	0.73	0.01
70	6.64	0.36	0.000	5.69	0.36	0.006	5.73	0.39		5.21	0.22		9.91	0.77	0.01
75	6.53	0.37	0.003	5.68	0.36	0.006	5.72	0.40		5.14	0.26	0.000	9.64	0.83	0.02
80	6.39	0.38	0.012	5.54	0.37	0.013	5.62	0.41		5.05	0.28	0.004	9.36	0.86	0.02
85	6.29	0.39	0.006	5.49	0.36	0.013	5.50	0.40	0.000	4.95	0.31	0.002	9.21	0.90	0.03
90	6.14	0.39	0.014	5.36	0.36	0.009	5.43	0.40	0.010	4.88	0.32	0.003	9.00	0.91	0.04
95	6.05	0.39	0.009	5.32	0.36	0.023	5.34	0.39	0.016	4.78	0.34	0.009	8.80	0.94	0.05
100	5.95	0.39	0.017	5.20	0.36	0.021	5.29	0.38	0.025	4.68	0.36	0.015	8.69	0.94	0.06
105	5.84	0.40	0.013	5.15	0.35	0.021	5.26	0.38	0.029	4.60	0.38	0.021	8.63	0.96	0.08
110	5.75	0.40	0.014	5.05	0.34	0.031	5.16	0.37	0.022	4.55	0.39	0.022	8.48	0.96	0.08
115	5.70	0.40	0.021	5.02	0.34	0.030	5.12	0.37	0.030	4.48	0.41	0.028	8.30	0.96	0.10
120	5.59	0.40	0.018	4.91	0.34	0.031	5.05	0.36	0.030	4.43	0.41	0.036	8.13	0.96	0.12
125	5.47	0.41	0.020	4.85	0.33	0.034	4.99	0.35	0.026	4.32	0.42	0.040	7.99	0.96	0.12
130	5.37	0.41	0.024	4.75	0.33	0.040	4.96	0.34	0.041	4.28	0.42	0.051	7.87	0.96	0.14
135	5.25	0.42	0.027	4.70	0.32	0.041	4.80	0.34	0.033	4.19	0.41	0.059	7.75	0.95	0.15
140	5.20	0.41	0.025	4.65	0.32	0.038	4.81	0.33	0.038	4.15	0.42	0.063	7.68	0.94	0.15
145	5.12	0.41	0.026	4.58	0.32	0.043	4.75	0.33	0.038	4.08	0.42	0.067	7.56	0.95	0.17
150	5.03	0.41	0.026	4.54	0.31	0.046	4.66	0.32	0.040	4.04	0.41	0.076	7.45	0.93	0.18
155	4.93	0.42	0.028	4.42	0.31	0.045	4.61	0.32	0.045	3.97	0.40	0.080	7.35	0.93	0.18
160	4.86	0.42	0.027	4.43	0.31	0.044	4.56	0.31	0.035	3.92	0.40	0.084	7.24	0.92	0.18
165	4.78	0.42	0.029	4.34	0.30	0.051	4.48	0.31	0.059	3.83	0.38	0.086	7.16	0.92	0.18
170	4.71	0.42	0.035	4.24	0.30	0.045	4.44	0.30	0.052	3.79	0.38	0.090	7.10	0.90	0.19
175	4.60	0.43	0.035	4.17	0.29	0.052	4.33	0.30	0.042	3.75	0.38	0.093	7.00	0.89	0.19
180	4.52	0.42	0.035	4.08	0.29	0.053	4.29	0.29	0.052	3.63	0.36	0.094	6.86	0.89	0.18
185	4.42	0.42	0.033	4.01	0.28	0.048	4.21	0.28	0.053	3.60	0.36	0.093	6.75	0.88	0.18
190	4.29	0.42	0.035	3.91	0.28	0.051	4.14	0.28	0.047	3.51	0.35	0.090	6.62	0.88	0.18
195	4.20	0.42	0.035	3.82	0.28	0.052	4.06	0.27	0.051	3.45	0.35	0.086	6.51	0.87	0.18
200	4.11	0.42	0.031	3.75	0.26	0.052	4.01	0.26	0.031	3.32	0.36	0.080	6.38	0.86	0.18

TABLE V. (Continued.)

	Sn ⁺	Sn ²⁺	Sn ³⁺	Sb ⁺	Sb ²⁺	Sb ³⁺	Te ⁺	Te ²⁺	Te ³⁺	Pb ⁺	Pb ²⁺	Pb ³⁺	Bi ⁺	Bi ²⁺	Bi ³⁺
5	0.00			0.00						0.04			0.07		
6	0.08			0.02						0.20			0.25		
7	0.37			0.13			0.00			0.83			0.76		
8	1.15			0.52			0.21			1.76			1.57		
9	2.19			1.16			0.71			2.59			2.50		
10	3.35			1.95			1.48			3.32			3.36		
11	4.49			2.77			2.27			3.91			4.03		
12	5.47			3.58			3.05			4.54			4.66		
13	6.28			4.35			3.72			5.16			5.33		
14	6.94			5.08			4.36			5.65			5.81		
15	7.49			5.67			4.94			6.07			6.21		
16	7.92			6.08			5.48			6.35			6.59		
17	8.31			6.42			6.02			6.59			6.85		
18	8.54			6.74			6.40			6.91			7.11		
19	8.80			7.07			6.66			7.25			7.36		
20	9.04			7.26			6.86			7.45			7.61		
21	9.18			7.49			7.12			7.55	0.00		7.67		
22	9.35			7.74			7.34			7.77	0.01		7.84		
23	9.47	0.00		7.83			7.41			7.93	0.01		8.15		
24	9.52	0.01		7.96	0.01		7.67			7.97	0.03		8.34	0.00	
25	9.55	0.04		8.08	0.02		7.90	0.00		8.04	0.05		8.39	0.01	
26	9.67	0.08		8.21	0.02		7.93	0.01		8.15	0.08		8.45	0.02	
27	9.75	0.12		8.26	0.04		7.96	0.01		8.20	0.11		8.53	0.04	
28	9.73	0.16		8.24	0.06		8.03	0.02		8.20	0.14		8.55	0.06	
29	9.73	0.17		8.30	0.08		8.13	0.02		8.16	0.17		8.66	0.08	
30	9.77	0.23		8.30	0.11		8.19	0.04		8.23	0.21		8.73	0.10	
32	9.74	0.30		8.32	0.17		8.27	0.08		8.32	0.28		8.73	0.17	
34	9.70	0.37		8.24	0.24		8.26	0.14		8.27	0.36		8.74	0.23	
36	9.65	0.43		8.23	0.30		8.14	0.20		8.26	0.43		8.75	0.30	
38	9.55	0.47		8.16	0.35		8.13	0.26		8.22	0.50		8.75	0.36	
40	9.52	0.51		8.08	0.40		8.25	0.32		8.25	0.56		8.76	0.42	
45	9.42	0.62		7.98	0.49		8.27	0.43		8.08	0.71		8.61	0.55	
50	9.24	0.72		7.84	0.55		8.22	0.51		7.95	0.84		8.51	0.68	
55	9.03	0.77		7.82	0.59		8.12	0.54		7.74	0.95		8.42	0.78	0.00
60	8.82	0.82		7.61	0.63	0.00	8.07	0.56	0.00	7.64	1.02		8.23	0.86	0.01
65	8.60	0.90	0.00	7.50	0.65	0.01	7.94	0.58	0.01	7.50	1.11	0.00	8.10	0.92	0.02
70	8.42	0.92	0.01	7.40	0.68	0.03	7.92	0.61	0.01	7.27	1.17	0.01	8.01	0.97	0.04
75	8.20	0.96	0.02	7.31	0.70	0.05	7.86	0.65	0.02	7.09	1.22	0.02	7.82	1.00	0.06
80	8.05	1.00	0.03	7.18	0.72	0.07	7.82	0.68	0.04	6.98	1.26	0.03	7.75	1.03	0.08
85	7.86	1.02	0.04	7.07	0.73	0.09	7.69	0.70	0.07	6.82	1.27	0.04	7.68	1.04	0.10
90	7.70	1.04	0.06	6.94	0.74	0.11	7.64	0.70	0.08	6.67	1.28	0.05	7.53	1.05	0.12
95	7.53	1.06	0.07	6.81	0.75	0.13	7.44	0.70	0.10	6.57	1.29	0.06	7.38	1.06	0.14
100	7.40	1.05	0.08	6.72	0.75	0.15	7.35	0.72	0.13	6.41	1.30	0.08	7.31	1.06	0.16
105	7.22	1.05	0.09	6.66	0.75	0.16	7.21	0.72	0.15	6.32	1.29	0.09	7.17	1.06	0.17
110	7.14	1.04	0.10	6.55	0.75	0.18	7.18	0.71	0.17	6.26	1.28	0.10	7.08	1.06	0.19
115	7.02	1.06	0.11	6.43	0.74	0.19	7.10	0.71	0.18	6.13	1.29	0.12	6.99	1.06	0.20
120	6.92	1.07	0.13	6.36	0.73	0.20	7.06	0.71	0.19	6.04	1.29	0.13	6.88	1.06	0.22
125	6.77	1.05	0.13	6.20	0.73	0.21	6.92	0.71	0.20	5.94	1.29	0.14	6.72	1.03	0.23
130	6.62	1.03	0.15	6.09	0.72	0.22	6.84	0.69	0.21	5.79	1.27	0.15	6.61	1.03	0.24
135	6.50	1.03	0.15	5.97	0.71	0.22	6.77	0.69	0.21	5.73	1.27	0.16	6.51	1.03	0.24
140	6.40	0.98	0.16	5.90	0.69	0.22	6.65	0.66	0.22	5.60	1.26	0.17	6.40	1.03	0.25
145	6.32	0.96	0.16	5.80	0.68	0.23	6.63	0.65	0.21	5.52	1.25	0.18	6.33	1.01	0.26
150	6.21	0.96	0.17	5.69	0.67	0.22	6.51	0.64	0.21	5.41	1.23	0.18	6.23	1.01	0.26
155	6.10	0.93	0.17	5.59	0.66	0.22	6.43	0.62	0.21	5.35	1.23	0.19	6.11	0.99	0.26
160	5.97	0.92	0.17	5.50	0.64	0.22	6.36	0.60	0.21	5.22	1.22	0.20	6.06	0.99	0.27
165	5.88	0.92	0.17	5.42	0.63	0.22	6.24	0.60	0.20	5.14	1.21	0.20	5.98	0.98	0.27
170	5.80	0.89	0.17	5.33	0.63	0.22	6.18	0.59	0.20	5.09	1.20	0.20	5.88	0.97	0.27
175	5.70	0.87	0.17	5.25	0.62	0.22	6.08	0.58	0.20	4.97	1.19	0.21	5.73	0.96	0.27
180	5.57	0.86	0.17	5.11	0.60	0.21	5.95	0.56	0.19	4.85	1.17	0.21	5.65	0.95	0.27
185	5.43	0.83	0.16	4.98	0.59	0.21	5.79	0.55	0.18	4.75	1.16	0.21	5.51	0.94	0.27
190	5.29	0.84	0.16	4.88	0.58	0.21	5.68	0.54	0.18	4.63	1.13	0.21	5.37	0.92	0.26
195	5.19	0.81	0.16	4.76	0.57	0.20	5.57	0.52	0.18	4.53	1.13	0.21	5.29	0.90	0.26
200	5.00	0.78	0.16	4.52	0.56	0.20	5.49	0.52	0.17	4.38	1.08	0.20	5.12	0.87	0.26

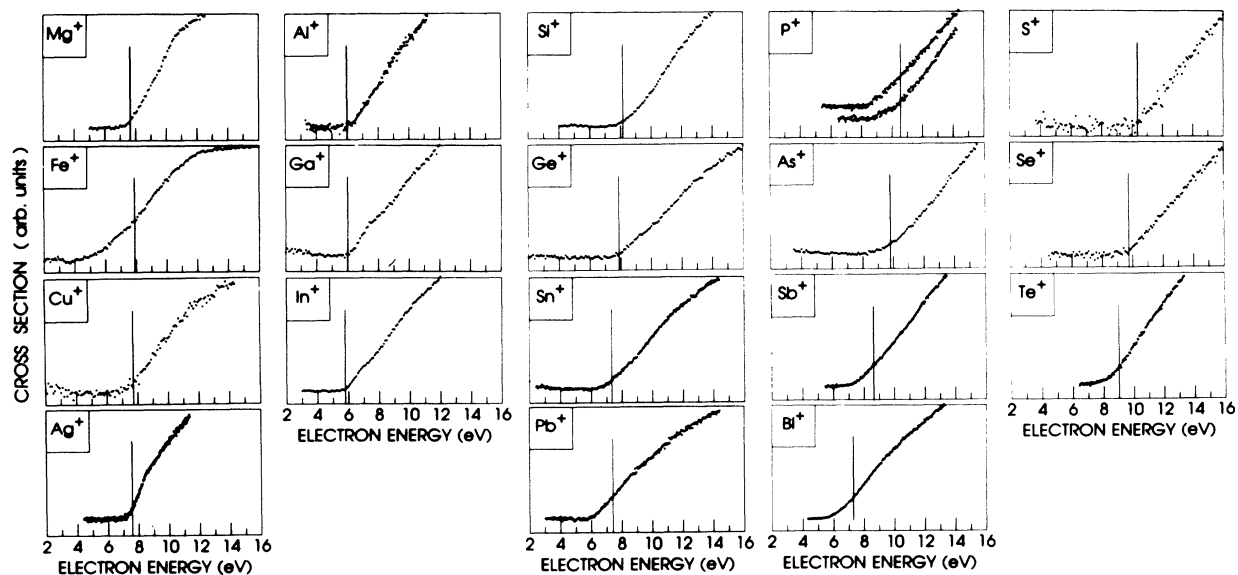


FIG. 6. Thresholds for single ionization. Vertical lines represent spectroscopic ionization potentials.

clearly shown by the P thresholds when it is formed by two different charge transfer gases; TEA gives predominantly the 2D excited state, whereas ethylene gives about equal amounts of the 4S ground state and 2D excited state. We expect the difference to be small between the ionization cross sections for the ground and these low-lying excited states, based on calculations using the Lotz theory (see below) and the fact that they have the same electron configurations, so we do not attempt to correct these cross sections.

Even though the energy resolution of these measurements is not high, there are observable bumps and breaks

near threshold for the Ag, Al, Ga, In, Si, Ge, Sn, and Pb atoms which suggest measurable contributions from excitation autoionization. Such behavior has been observed and analyzed before for Ga,⁴⁸ In,^{48,65,66} Ag,⁶⁷ Sn,⁶⁵ and Pb.³⁵ Even in cases where the structure is not resolved, the existence of a large number of autoionizing states could increase the magnitudes of the apparently smooth cross sections.

The threshold regions for double ionization are shown in Fig. 7. All thresholds lie at or close to the energy for double ionization, verifying that the detected species are indeed the doubly charged ions. Although the signal-to-

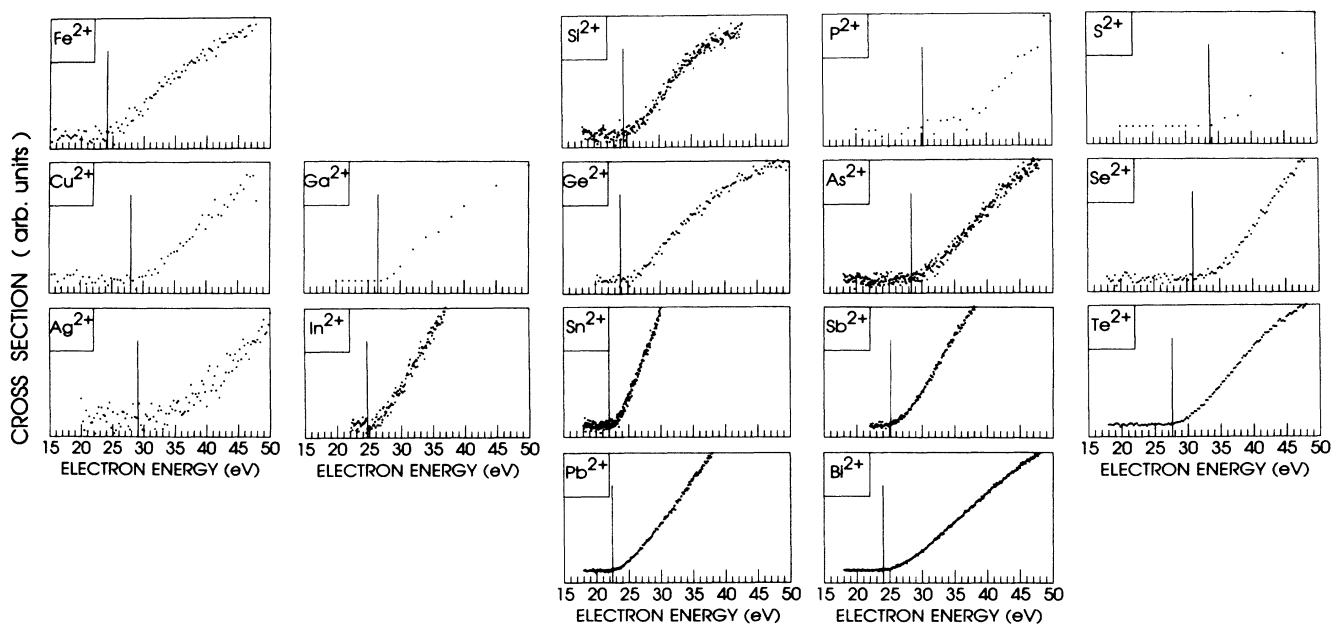


FIG. 7. Thresholds for double ionization.

noise ratio is too small to permit definitive analyses, most of these double-ionization thresholds appear to increase quadratically with energy above threshold, in accordance with theories of threshold behavior for direct double ionization. The Fe, Ga, and In atoms, however, have thresholds which appear to increase linearly. The Fe data could be distorted by the many states in the beam. The Ga and In data suggest that double ionization of these atoms is dominated by autoionization.^{42,48}

Triple ionization is too weak for meaningful thresholds to be measured, except for four of the heaviest atoms Sb, Te, Pb, and Bi (Fig. 8). The interpretation is complicated because all four of these neutral atom beams contain excited states. Nevertheless, all of the measurable intensity is above the triple IP, verifying that the detected species are the triple ions. Although the signal-to-noise ratio is too small to permit definitive analyses, most of these triple-ionization thresholds appear to increase as the cube of the excess energy, suggesting that they are dominated by direct triple ionization rather than indirect processes such as single inner-shell ionization followed by double autoionization, or direct double ionization followed by autoionization.

IV. DISCUSSION

A. Single ionization

The measured cross sections in Fig. 5 and Table V are compared to each other across rows of the Periodic Table in Fig. 9, and down columns in Fig. 10. Cross sections of the halogen and rare-gas atoms from previous work^{13,47} are included in Figs. 9 and 10, along with accurate measurements of the C, N, and O cross sections from Brook, Harrison, and Smith.¹²

The single-ionization comparisons in Fig. 9 reveal monotonic decreases across the rows and those in Fig. 10 show monotonic increases down the columns. The monotonic trends in Figs. 9 and 10 tend to corroborate the estimated relative measurement accuracy of 7%. If the accuracy were much less for these independent measurements, we would expect less regular variations across rows and down columns. The magnitude of the Al cross section is somewhat disturbing, however, since it is even larger than $\sigma(\text{Ga})$. Nevertheless, it did reproduce on two

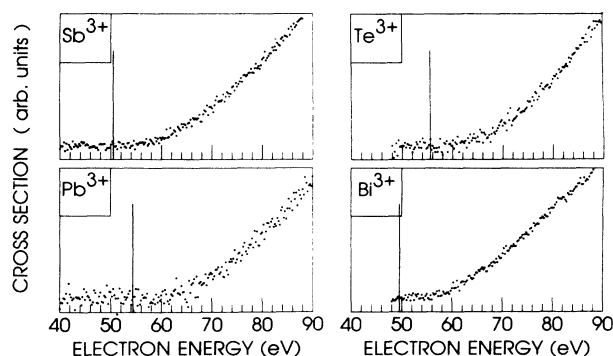


FIG. 8. Thresholds for triple ionization.

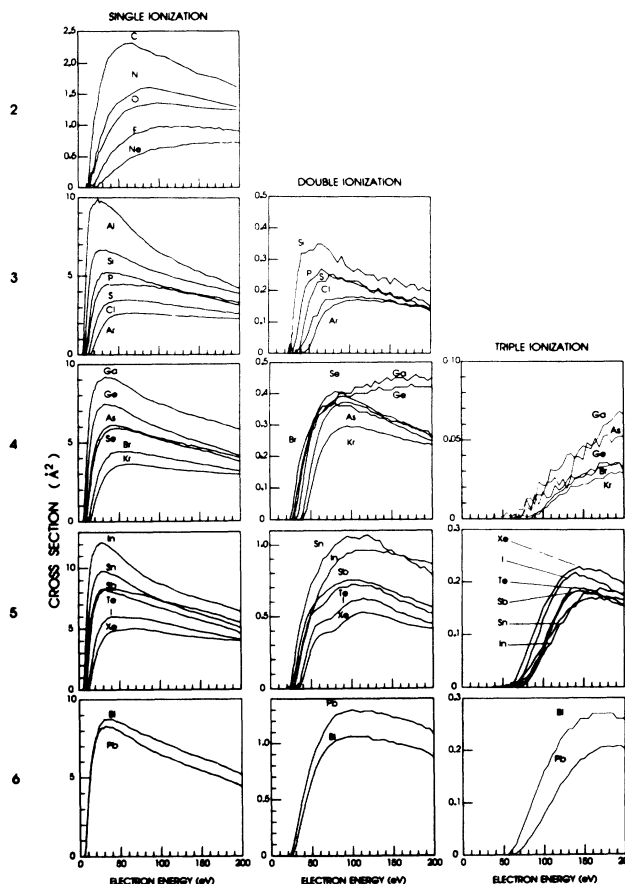


FIG. 9. Comparisons of measured cross sections across the rows of the Periodic Table.

different days with two different sources. Similarly, it is surprising that $\sigma(\text{Pb})$ is smaller than $\sigma(\text{Sn})$. There is a hint of similar behavior in the neighboring column, where $\sigma(\text{Bi})$ is only slightly larger than $\sigma(\text{Sb})$.

None of the cross sections show any gross structure, but some differences in shape are apparent. The most noticeable shape differences are for the cross sections of the group VIA atoms S, Se, and Te, which fall off more slowly than those of the neighboring group VA atoms and so cross them at higher energies. Although the cross section for the lightest group VIA atom O does not cross $\sigma(\text{N})$, they are closer together than those for the other atoms in row 2.

Cross sections for the group IIIA atoms Al, Ga, and In show decreases in slope for energies above 100 eV, that is, they are concave upward. Looking across the top row of Fig. 10, it is clear that the cross sections become less concave, and by group VIA are convex upward. This behavior may be related to changes in the relative intensity of two peaks; the higher one is seen most prominently in Xe, and is resolved in I and Te.

Almost all of the single-ionization cross sections measured here peak between 3.3 and 5.7 times the threshold energy. The main exceptions are Mg, which peaks at only 2.6 times threshold, and Ag, which peaks at 6.0

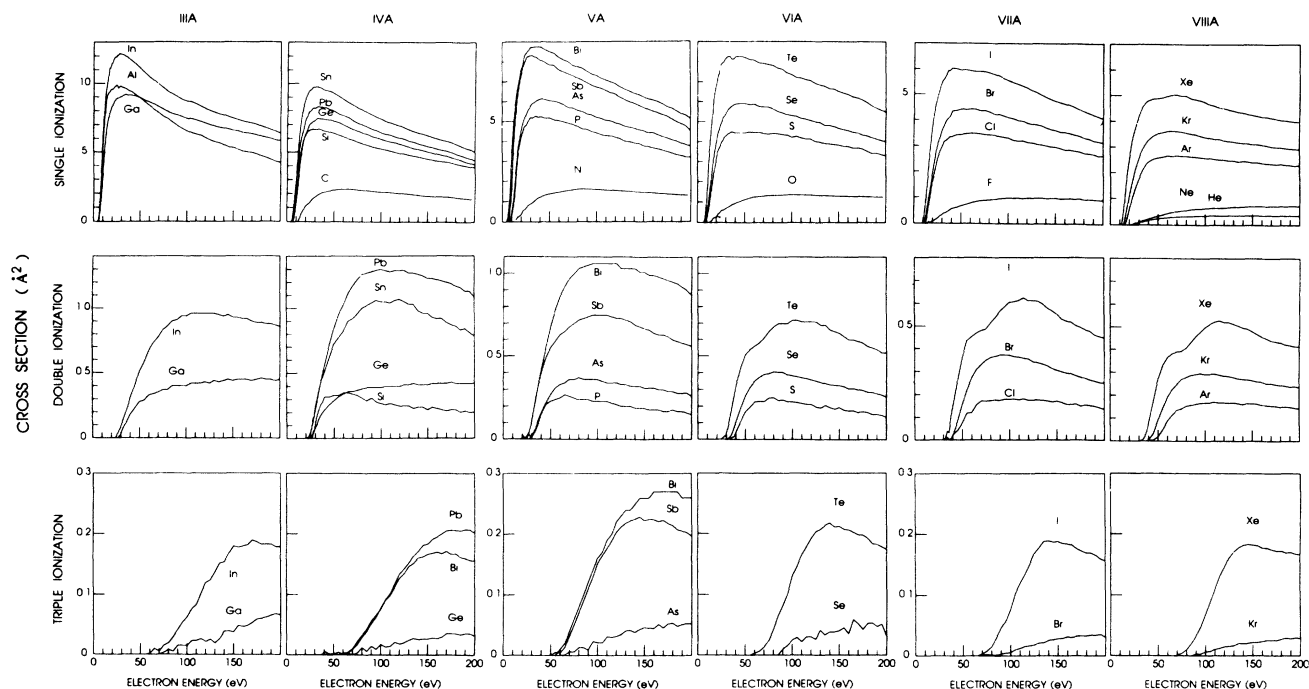


FIG. 10. Comparisons of measured cross sections down the columns of the Periodic Table.

times threshold, possibly due to a contribution from ionization of $4d$ electrons.

B. Double and triple ionization

The cross-section data for double ionization are less complete than for single ionization since the signals are weaker and noisier. Nevertheless, several trends are apparent in Figs. 9 and 10. As for single ionization, the double-ionization cross sections tend to decrease going from group IIIA to group VIIIA, and increase going down the columns. Another interesting trend is the giant resonance⁶⁸ due to the $4d$ orbital,⁶⁹ which had been seen before in Xe and I; it appears also in Te, and possibly in Sb.

Most of the double-ionization cross sections peak at 2–3 times threshold. Exceptions are Cu (Fig. 5), Ga, and Ge, which continue to increase up to 200 eV, roughly 6 times threshold, and In, which does not fall as rapidly as other atoms in row 5. These atoms have d orbitals with low ionization potentials, so this behavior may reflect the involvement of d electrons in ionization autoionization.

The data for triple ionization are even more noisy and more limited than those for double ionization (Figs. 9 and 10). The data for the row 4 atoms are particularly noisy not only because the cross sections are smaller than those of row 5 but also because the background is larger. They do not peak by 200 eV, the maximum energy measured here. The row 5 cross sections peak at lower energies, about 150 eV, and are remarkably similar in magnitude.

C. Comparison to previous measurements

Cross sections have been measured before for only 8 of the 18 atoms measured here. Previous results for those eight are compared in Fig. 11 and Table VI to the present results. Whereas our previous measurements¹³ with this apparatus of the rare-gas ionization cross sections agreed within $\pm 15\%$ with well-accepted values, agreement for other atoms of previous results with our present measurements is generally worse; the previous values range from half to almost twice our present results. Shapes also differ considerably, with some peaks at different energies and with different rates of falloff at energies higher than the peak. Some of the previous shapes show structure and threshold energies which are hard to understand, especially for Cu, Ag, Al, Ga, and In. The shape differences must result from a variety of causes, difficult to identify from the available information. Only 7 of the 18 previous measurements have shapes which agree reasonably well with the present measurements (Table VI).

A number of measurements have been made of the ratio between two cross sections at a single electron energy, using the ion source of a mass spectrometer.^{70–80} Table VII lists those directly measured ratios of atomic total ionization cross sections, omitting ratios which requires the assumption that the atomic cross section is some particular fraction of a measured molecular cross section. For three of the listed ratios $\sigma(\text{Fe})/\sigma(\text{Ag})$, $\sigma(\text{Sn})/\sigma(\text{Cu})$, and $\sigma(\text{Sn})/\sigma(\text{Ag})$, cross sections for both of the atoms were also measured in this work. The agreement shown in Table VII is moderately good. We use the other ratios

TABLE VI. Ratio of peak ionization cross sections of previous measurements to present measurements.

Atom	Ratio or peak cross sections previous/present	Reference	Shape of previous cross section
He	1.0	11	Agrees
Ne	1.0	11	Agrees
Ar	1.0	11	Agrees
Kr	1.0	11	Agrees
Xe	0.82	11	Agrees
Mg	0.79	31	Agrees
Mg	1.71	28	Agrees
Mg	1.71	27	Same peak energy. Falls faster.
Mg	1.47	29,30	Peak energy lower. Falls faster.
Cu	0.75	35	Agrees
Cu	1.0	37,38	Peak energy higher.
Cu	1.87	46	Peak energy higher.
Ag	0.83	39	Peak energy higher. Falls faster.
Ag	0.51	35	Peak energy lower.
S	0.73	44	Agrees
Al	0.52	42	Agrees
Al	0.69	40,41	Peak energy higher.
Ga	0.66	43	Peak energy lower. Falls faster.
Ga	0.75	40,41	Peak energy higher.
In	0.61	43	Peak energy lower. Falls faster.
In	0.65	40,41	Peak energy higher. Weak peak lower.
Pb	0.73	35	Agrees
Pb	0.73	36	Agrees

TABLE VII. Ratios of total ionization cross sections from mass spectrometer measurements.

$\sigma(X)/\sigma(Y)$	Energy (eV)	Ratio	Reference	Ratio from this work
Zn/Te	70	0.48	70	
Cd/Zn	50	1.68	71	
Be/O	70	2.1	72	
B/Ag	50-70	0.15±0.05	73	
Fe/Ag	60	0.97	74	0.84
Co/Ag	60	1.13	74	
Ni/Ag	60	0.95	74	
Fe/Co	60	0.89	74	
Ni/Co	60	0.85	74	
Ni/Fe	60	1.00	74	
Cr/Au	70	1.5±0.4	75	
Ti/B	40	7.6±1.5	76	
Au/Cu	^a	1.90	77	
Au/Cu	70	2.12	80	
Au/Cu	70	2.0±0.2	38	
Sn/Cu	70	3.42	75	2.79
Sn/Ag	70	1.81	75	1.82
Sn/Au	70	1.62	75	
S/U	50	0.41±0.14	78	
U/Ag	^a	1.44	79	

^aNot given. Presumed to be 70 eV.

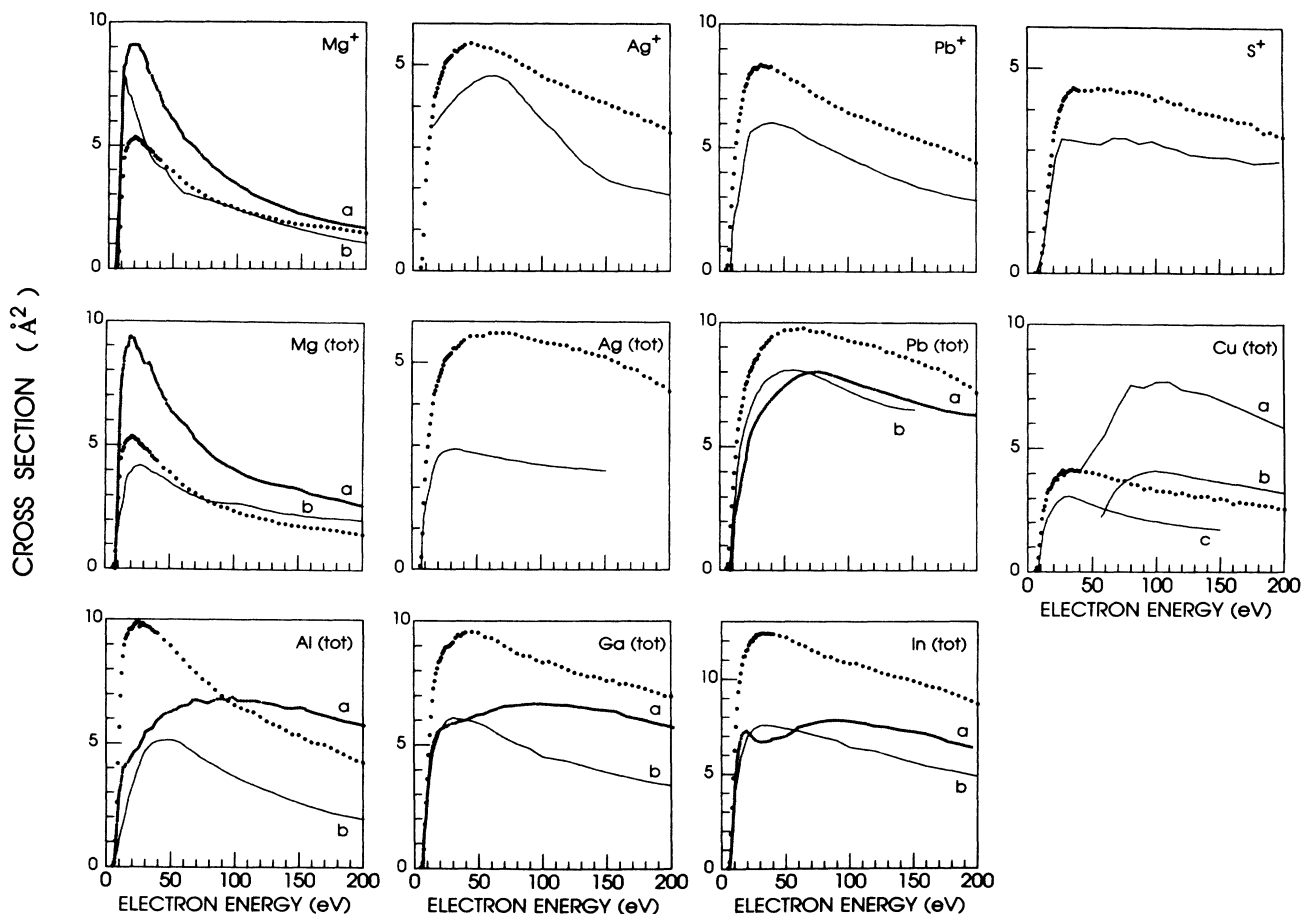


FIG. 11. Comparisons of present and previous cross-section measurements for single and total ionization. For all atoms, the heavy dots are the present results. Previous results (solid lines) for Mg^+ are from (a) Ref. 28, (b) Ref. 30; $Mg(tot)$ from (a) Ref. 27, (b) Ref. 31; Ag^+ from Ref. 39; $Ag(tot)$ from Ref. 34; Pb^+ from Ref. 34; $Pb(tot)$ from (a) Ref. 36, (b) Ref. 34; S^+ from Ref. 44; $Cu(tot)$ from (a) Ref. 38, (b) Ref. 37, (c) Ref. 34; $Al(tot)$ from (a) Refs. 40 and 41; (b) Ref. 42; $Ga(tot)$ and $In(tot)$ from (a) Refs. 40 and 41, (b) Ref. 43.

in Table VII and the present data to derive total ionization cross sections for nine other atoms at a single energy, mostly 70 eV (Table VIII). The derived value for Sn is only 17% larger than the value measured here. The value for Au fits well with an increasing trend down the IB column. The value for B is much too small to fit the smooth trend in Fig. 9 and so is suspect. Consequently, the Ti value is also likely to be too small since it is derived from the B value.

Comparisons of the double- and triple-ionization cross sections to previous measurements are shown in Fig. 12 for Cu, Ag, S, Ga, In, and Pb. Our ratio of $\sigma(S^{2+})/\sigma(S^+)$ agrees well with that of Ziegler *et al.*,⁴⁴ but our magnitudes for both double and single ionization are about 30% larger. Our double-ionization cross sections for Ga and In agree remarkably well with those of Golovach *et al.*⁴² considering the 30% differences for single ionization. Our cross sections for formation of Pb^{2+} and Pb^{3+} agree well with previous data,³⁴ but our values for Cu^{2+} and Ag^{2+} are smaller by a factor of 2 or more

than those reported previously.³⁷⁻³⁹

In our previous rare-gas measurements we noted that the Xe cross section was 12% larger than the value reported by REG.¹¹ We argued there that this difference may be significant because Xe was the rare gas which could be measured with the best signal-to-noise ratio in our apparatus, while REG's pressure measurement is expected to be least accurate for Xe. This difference, while not large, is important since the rare gases are so conveniently and so frequently used as references, and REG's measurements are often considered to be the most accurate. Remeasurement of the Xe single-ionization cross section in this work yields a value of $5.37 \pm 0.54 \text{ \AA}^2$ at 70 eV. This is 24% larger than REG's value of 4.33 \AA^2 for single ionization (obtained by subtracting the double- and triple-ionization cross sections¹³ from their total ionization cross section). It is also larger than the $4.96 \pm 0.74 \text{ \AA}^2$ value reported by Ref. 13, but well within the experimental uncertainty. Additional comparisons to previous work given in Table IX are the ratios of Xe to

Ar and Xe to Kr total ionization cross sections measured by other workers; these ratios are in remarkably good agreement, and strongly support the larger value for the Xe cross section. Given these results, we suggest that the most accurate available total ionization cross section for Xe at any energy is the value given by REG,¹¹ increased by a factor of 1.17.

D. Comparison to theory

Efforts to calculate atomic ionization cross sections began before the quantum theory was formulated, with theories based on classical mechanics. Even now there is no adequate quantum-mechanical method to calculate ionization cross sections of neutral atoms; calculations at

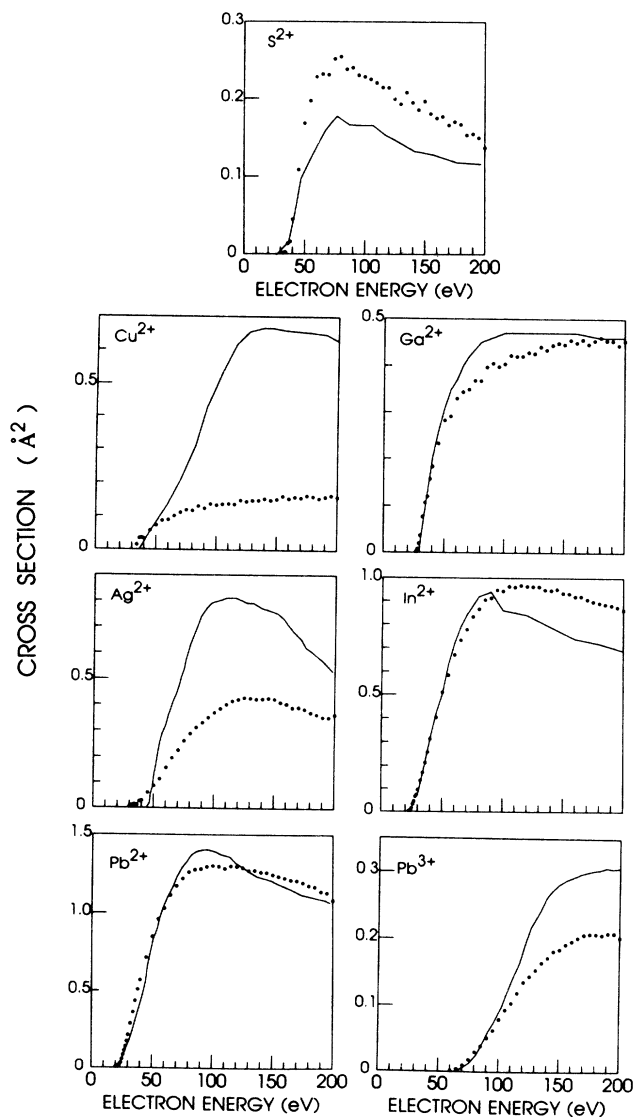


FIG. 12. Comparisons of present and previous measurements of double- and triple-ionization cross sections. For all atoms, the heavy dots are the present results. Previous results (solid lines) for S^{2+} are from Ref. 44; Cu^{2+} from Ref. 37; Ag^{2+} from Ref. 39; Pb^{2+} from Ref. 34; Pb^{3+} from Ref. 34; Ga^{2+} from Ref. 43; In^{2+} from Ref. 43.

TABLE VIII. Total ionization cross sections (at 70 eV) from the literature or derived from literature ratios and the present measurements.

Atom	Total cross section	Derivation	Comparisons
Ag	5.65 ^a		
Cd	8.54 ^b		
Cu	3.69 ^a		
Fe	4.76 ^a		
Hg	9.4 ^c		
O	1.30 ^d		
S	4.87 ^a		
Se	6.51 ^a		
Sn	10.28 ^a		
Te	9.17 ^a		
Zn	5.03 ^b		
Au ^e	7.01	1.90 $\sigma(Cu)$	
Au ^e	7.82	2.12 $\sigma(Cu)$	
Au ^e	7.38	2.0 $\sigma(Cu)$	
B	0.85	0.15 $\sigma(Ag)$	
Be	2.73	2.1 $\sigma(O)$	
Co ^f	6.38	1.13 $\sigma(Ag)$	
Co ^f	5.35	1.12 $\sigma(Fe)$	
Cr	11.12	1.5 $\sigma(Au)$	
Ni ^g	5.37	0.95 $\sigma(Ag)$	
Ni ^g	4.76	1.00 $\sigma(Fe)$	
Sn	12.01	1.62 $\sigma(Au)$	10.28 ^a
Ti	6.44	7.6 $\sigma(B)$	
U	11.88	2.44 $\sigma(S)$	7.66 ^h

^aFrom this work.

^bReference 71.

^cReference 4.

^dReference 12.

^eAverage $\sigma(Au) = 7.40$.

^fAverage $\sigma(Co) = 5.87$.

^gAverage $\sigma(Ni) = 5.04$.

^hReference 46.

low energy are often in error by a factor of 2. Although ionization is conceptually straightforward, the exit channel involves three charged particles (or more, for multiple ionization). Present quantum theory is quantitatively accurate only in the high-energy limit, whereas cross sections are largest and much important physics takes place for electron energies less than 10 times threshold.

In the absence of measurements or of accurate quantum-mechanical theory, users of single-ionization cross-section data have often turned to approximate classical theories,^{81,82} to the Born approximation,⁸³ or to semiempirical fits based on the limited available data.⁸⁴⁻⁸⁶ These approaches are of poorly known accuracy because few accurate measurements exist for calibration or testing. Here we use the present experimental results to check the predictions of five of these calculations. Figures 13-15 compare the maximum cross sections measured in this work to the maximum cross sections from each of these calculations.

Gryzinski⁸² used a modification of Thomson's classical

TABLE IX. Experimental values of the Xe total ionization cross section (\AA^2) at 70 eV, based on ratios from the literature and Ar and Kr cross sections from Table II.

$\frac{\sigma_T(\text{Xe})}{\sigma_T(\text{Ar})}$	$\frac{\sigma_T(\text{Xe})}{\sigma_T(\text{Kr})}$	$\sigma_T(\text{Xe})^a$	$\sigma_T(\text{Xe})^b$	Reference
1.85	1.22	5.37	5.12	11
2.10	1.42	6.09	5.96	58
2.21	1.40	6.5	5.91	60
2.07	1.42	6.01	5.94	61
2.15	1.45	6.24	6.09	62
2.15	1.42	6.24	5.96	63
2.01	1.30	5.83	5.46	64
1.98	1.38	5.75	5.80	13
Average =		6.09 ± 0.25^c	5.87 ± 0.20^c	
Combined average =			5.98 ± 0.25	
$\sigma_T(\text{Xe})$ this work =			6.22 ± 0.54	

^aBased on $\sigma_T(\text{Ar}) = 2.90 \text{\AA}^2$.

^bBased on $\sigma_T(\text{Kr}) = 4.20 \text{\AA}^2$.

^cOmits data from Ref. 11.

binary encounter theory⁸¹ to derive a straightforward formula for the contribution of each orbital to the cross section. Otvos and Stevenson⁸⁴ assumed that the maximum cross section is given by the weighted sum of the mean-square radii of the valence electrons. Mann⁸⁵ improved on this by considering the variation with energy of the cross section for each orbital and by using Hartree-Fock wave functions to calculate the mean-square radii. Lotz⁸⁶ derived a semiempirical formula which has become quite popular and appears to be moderately accurate for direct ionization of singly and multicharged ions. McGuire⁸³

scaled Born approximation calculations to experimental data to derive parametrized formulas.

To calculate cross sections in Figs. 13–15 from the theories of Gryzinski and Lotz, we include the three outermost orbitals and take orbital energies from Lotz.⁸⁷ It is clear that there are important differences between experiment and the results of these calculations. Most noticeable is that the variation of experimental cross sections from column IIIA to column VIIIA (Fig. 13) is greater than the predictions of any of the theories. Trends down columns of the Periodic Table are predicted

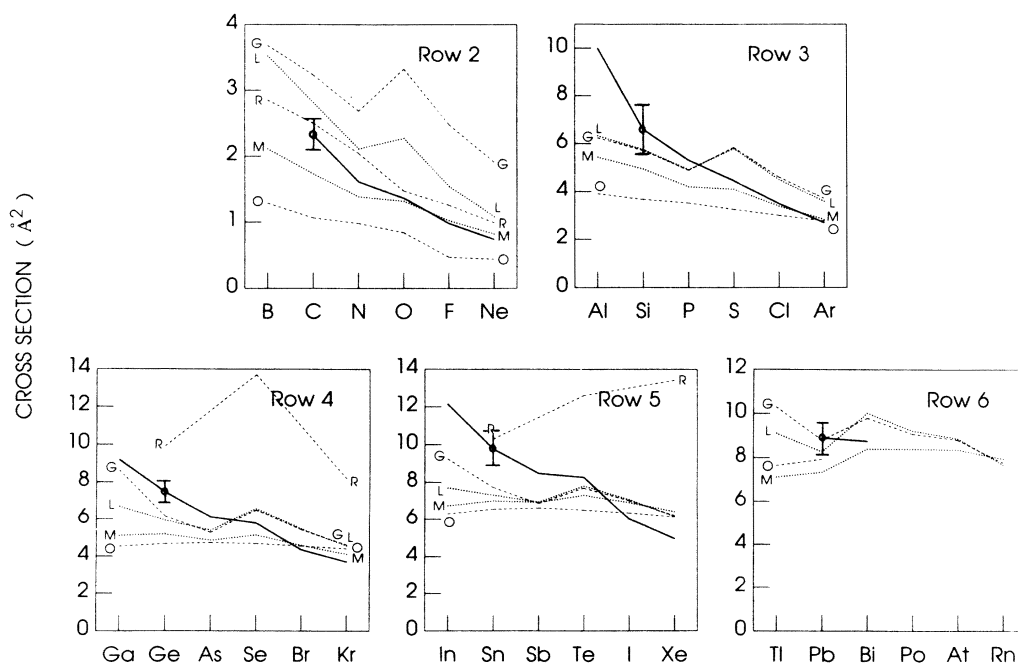


FIG. 13. Comparisons of peak cross sections from these measurements (—) to the predictions of Gryzinski (G), Lotz (L), Mann (M), Otvos and Stevenson (O), and McGuire (R) for the atoms in rows 2–6.

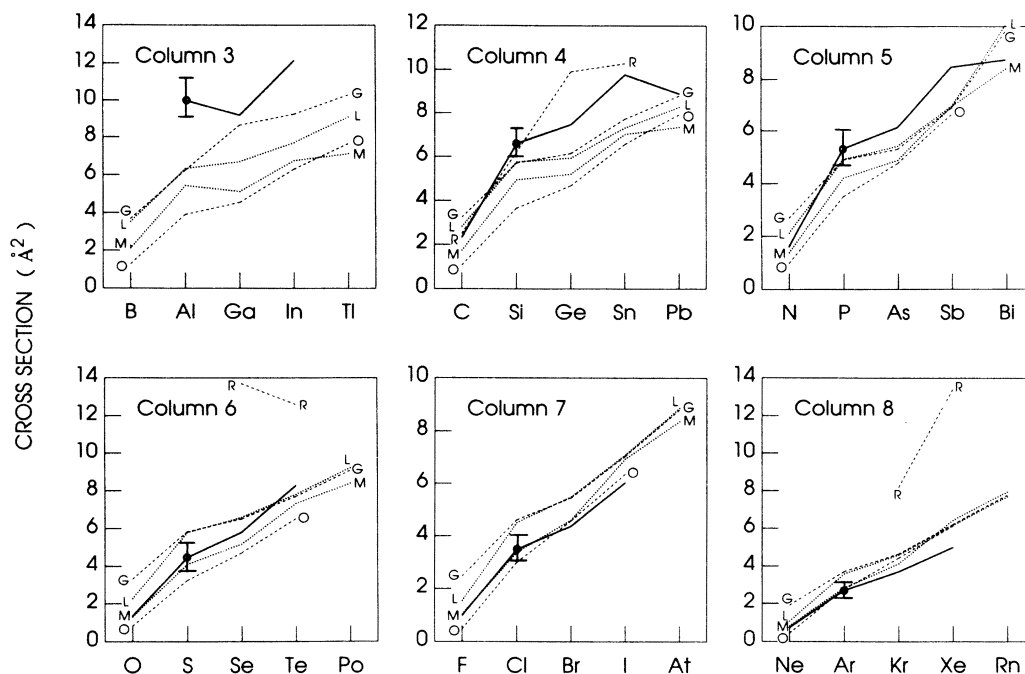


FIG. 14. Comparisons of peak cross sections from these measurements (—) to the predictions of Gryzinski (G), Lotz (L), Mann (M), Otvos and Stevenson (O), and McGuire (R) for the atoms in columns IIIA–VIIIA.

better by the various theories (Fig. 14). This large variation across the rows might result in part from the omission of autoionization by all of the theories. It could also result from the effects of the ns and $(n-1)d$ electrons. These orbitals are loosely bound in the group IIIA atoms and must contribute to their ionization cross sections, but lie deeper and contribute little or nothing to the cross sections of atoms in groups VA–VIIIA. It is also interesting that the Gryzinski values for Fe, Cu, and Ag (Fig. 15) lie so much above both experiment and the other theories. This too could result from an incorrect treatment of ionization of d electrons. The discontinuity observed between columns VA and VIA (Fig. 9) is predicted best by the Gryzinski and Lotz theories (Fig. 13). Its ori-

gin appears to be the near equality of ionization potentials for columns VA and VIA, which breaks the otherwise monotonic increase of ionization potentials across each row. This effect occurs because electrons go into different orbitals (p_x, p_y, p_z) until p^4 , when two electrons must be paired in the same orbital, raising the total energy of the atom, lowering the ionization potential, and raising the ionization cross section.

Otvos and Stevenson, and Mann calculate only the maximum cross section, but the other three also calculate shapes as a function of energy. These shapes (not shown in this paper) tend to agree with experiment, peaking at about 4 times threshold, but the differences are far beyond experimental error.

V. CONCLUSIONS

The differences between our cross sections and many of the previous measurements, especially our large values for single ionization of column IIIA and IVA atoms, force us to examine once more the accuracy ($\pm 7\%$ relative uncertainties) of our measurements. Since our values are relative to Ar and Kr, the potential errors to examine are those which would affect different atoms differently. Errors related to the electron beam such as electron reflection, secondary electrons, and overlap need not be considered since they should be independent of atom. Almost every potential source of error we can identify would, if present, tend to lower our reported cross sections. The reported cross sections are lowered, for example, if ions fail to reach the detector, if the neutral beam is contaminated with impurity atoms (almost all of which would have smaller cross sections than the atoms mea-

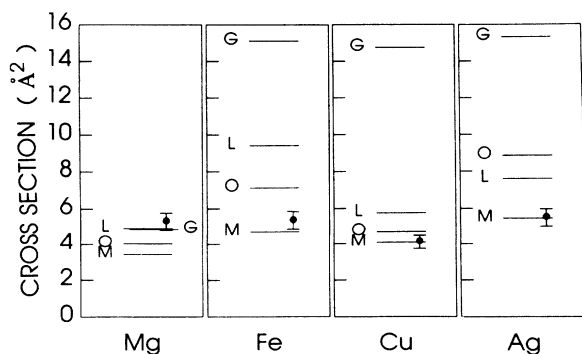


FIG. 15. Comparisons of peak cross sections from these measurements (●) to the predictions of Gryzinski (G), Lotz (L), Mann (M), Otvos and Stevenson (O), and McGuire (R) for Mg, Fe, Cu, and Ag.

sured here), if infrared radiation from the ion source gives an erroneously large value for the neutral-beam flux, if the CEM efficiency is less than 0.96, or if some ions observed by other experimenters form only by slow autoionization after a time long compared to our time of flight to the hemispherical analyzer. The only error we have identified which would give an erroneously large cross section is the possibility that thermal ions are trapped by space charge in the electron beam and, by charge transfer, create fast ions indistinguishable from signal. To prevent this possibility, all of these measurements have been made with a 3-V/cm electric field across the collision region, to sweep out any thermal ions. Trapped ions thus are apparently unimportant, since cross sections measured with this field turned off are the same as those made with it on. We conclude that if any of these errors are present but unaccounted for, our reported cross sections would be smaller than the correct values; the correction of any of these errors would increase the disagreement between this work and many of the previous measurements or theory.

In summary, single-ionization cross sections for the 16 atoms measured here have $\pm 10\%$ uncertainties. The shapes offer few surprises, generally having single peaks near 4 times the threshold energy. The peak magnitudes from column IIIA to column VIIIA decrease nearly monotonically, and vary more than predicted by various approximate theories. Agreement with previous measurements for eight atoms is generally poor, with peak cross sections differing from 30% to 100%.

It is clear that improved theory is needed. Semiempiri-

cal theories could use the present data for better fits. Autoionization needs to be considered. The role of d orbitals in particular needs to be treated more accurately.

For a variety of reasons, many atoms were not measured in this work. For some, such as the alkali-metal and alkaline-earth atoms (except for Mg) and most of the transition metals, no suitable charge-transfer gases could be found with low enough ionization potentials. Alkali-metal vapors would probably have been successful, but we avoided using them since they might have contaminated the vacuum chamber. For many transition metal and rare-earth atoms, an intense enough ion beam could not be obtained from the Colutron ion source. Other atoms such as Zn, Cd, and Hg were avoided since they might have contaminated the vacuum chamber. All of these atoms could probably be studied by this method, with suitable modifications to the apparatus. For some, however, forming a pure ground-state beam could be difficult, as shown by the present data on Fe.

ACKNOWLEDGMENTS

We thank Professor T. Moran for suggesting the use of triethylamine as a charge-transfer gas; F. A. Baiocchi, P. B. Armentrout, and S. M. Tarr for contributions to the design of this apparatus; G. Dunn, S. Younger, and D. Gregory for discussions of the theory; and R. Sherwood, T. Kometani, S. Zahurak, M. Mandich, T. DeSantolo, M. Steigerwald, and D. S. Williams for providing us with source materials.

-
- ¹P. T. Smith, *Phys. Rev.* **36**, 1293 (1930).
²W. Bleakney, *Phys. Rev.* **34**, 157 (1929); **35**, 139, 1180 (1930); **36**, 1303 (1930); **37**, 808 (1931).
³K. T. Compton and I. Langmuir, *Rev. Mod. Phys.* **2**, 123 (1930).
⁴L. J. Kieffer and G. H. Dunn, *Rev. Mod. Phys.* **38**, 1 (1966).
⁵*Electron Impact Ionization*, edited by T. D. Märk and G. H. Dunn (Springer-Verlag, New York, 1985).
⁶R. S. Freund, in *Swarm Studies and Inelastic Electron-Molecule Collisions*, edited by L. C. Pitchford, B. V. McKoy, A. Chutjian, and S. Trajmar (Springer-Verlag, New York, 1987).
⁷H. Tawara and T. Kato, *At. Data. Nucl. Data Tables* **36**, 167 (1987).
⁸K. L. Bell, H. B. Gilbody, J. G. Hughes, A. E. Kingston, and F. J. Smith, *J. Phys. Chem. Ref. Data* **12**, 891 (1983).
⁹M. A. Lennon, K. L. Bell, H. B. Gilbody, J. G. Hughes, A. E. Kingston, M. J. Murray, and F. J. Smith, *J. Phys. Chem. Ref. Data* **17**, 1285 (1988).
¹⁰G. H. Dunn, in *Electron Impact Ionization* (Ref. 5), p. 277.
¹¹D. Rapp and P. Englander-Golden, *J. Chem. Phys.* **43**, 1464 (1965).
¹²E. Brook, M. F. A. Harrison, and A. C. H. Smith, *J. Phys. B* **11**, 3115 (1978).
¹³R. C. Wetzal, F. A. Baiocchi, T. R. Hayes, and R. S. Freund, *Phys. Rev. A* **35**, 559 (1987).
¹⁴J. Fletcher and I. R. Cowling, *J. Phys. B* **6**, L258 (1973).
¹⁵M. V. Kurepa, I. M. Cadez, and V. M. Pejcev, *Fizika (Zagreb)* **6**, 185 (1974).
¹⁶M. B. Shah, D. S. Elliot, and H. B. Gilbody, *J. Phys. B* **20**, 3501 (1987).
¹⁷E. C. Zipf, *Planet. Space Sci.* **33**, 1303 (1985).
¹⁸G. O. Brink, *Phys. Rev.* **127**, 1204 (1962).
¹⁹R. H. McFarland and J. D. Kinney, *Phys. Rev.* **137**, A1058 (1965).
²⁰I. P. Zapesochnyi and I. S. Aleksakhin, *Zh. Eksp. Teor. Fiz.* **55**, 76 (1968) [*Sov. Phys.—JETP* **28**, 41 (1969)].
²¹R. Jalin, R. Hagemann, and R. Botter, *J. Chem. Phys.* **59**, 952 (1973).
²²G. O. Brink, *Phys. Rev.* **127**, 1204 (1962); **34**, A345 (1964).
²³K. J. Nygaard, *Phys. Lett.* **51A**, 171 (1975).
²⁴K. J. Nygaard and Y. B. Hahn, *J. Chem. Phys.* **58**, 3493 (1973).
²⁵H. Heil and B. Scott, *Phys. Rev.* **145**, 279 (1966).
²⁶K. J. Nygaard, *J. Chem. Phys.* **49**, 1995 (1968).
²⁷Y. Okuno, K. Okuno, Y. Kaneko, and I. Kanomata, *J. Phys. Soc. Jpn.* **29**, 164 (1970).
²⁸S. Okudaira, Y. Kaneko, and I. Kanomata, *J. Phys. Soc. Jpn.* **28**, 1536 (1970).
²⁹F. Karstensen and M. Schneider, *Z. Phys. A* **273**, 321 (1975).
³⁰F. Karstensen and M. Schneider, *J. Phys. B* **11**, 167 (1978).
³¹L. A. Vainshtein, V. I. Ochkur, V. I. Rakhovskii, and A. M. Stepanov, *Zh. Eksp. Teor. Fiz.* **61**, 511 (1971) [*Sov. Phys.—JETP* **34**, 271 (1972)].
³²R. H. McFarland, *Phys. Rev.* **159**, 20 (1967).
³³Y. Okuno, *J. Phys. Soc. Jpn.* **31**, 1189 (1971).
³⁴S. I. Pavlov, and G. I. Stotskii, *Zh. Eksp. Teor. Fiz.* **58**, 108

- (1970) [Sov. Phys.—JETP **31**, 61 (1970)].
- ³⁵S. I. Pavlov, V. I. Rakhovskii, and G. M. Fedorova, *Zh. Eksp. Teor. Fiz.* **52**, 21 (1967) [Sov. Phys.—JETP **25**, 12 (1967)].
- ³⁶D. G. Golovach, V. I. Rakhovskii, and V. M. Shustryakov, *Prib. Tekh. Eksp.* **6**, 141 (1986) [Instrum. Exp. Tech. (USSR) **29**, 1396 (1987).]
- ³⁷C. K. Crawford, as reported by L. J. Kieffer, *At. Data* **1**, 19 (1969).
- ³⁸J. M. Schroerer, D. H. Gündüz, and S. Livingston, *J. Chem. Phys.* **58**, 5135 (1973).
- ³⁹C. K. Crawford and K. I. Wang, *J. Chem. Phys.* **47**, 4667 (1967).
- ⁴⁰I. P. Zapesochnyi, J. E. Kontros, and L. L. Shimon, in *Abstracts of the Ninth International Conference on the Physics of Electronic and Atomic Collisions, Seattle, 1975*, edited by J. S. Risley and R. Geballe (University of Washington Press, Seattle, 1975), p. 900.
- ⁴¹L. L. Shimon, E. I. Nepipov, and I. P. Zapesochnyi, *Zh. Tekh. Fiz.* **45**, 688 (1975) [Sov. Phys.—Tech. Phys. **20**, 434 (1975)].
- ⁴²D. G. Golovach, A. N. Drozdov, V. I. Rakhovskii, and V. M. Shustryakov, *Izmer. Tekh.* **6**, 51 (1987) [Meas. Tech. (USSR) **30**, 587 (1987)].
- ⁴³L. A. Vainshtein, D. G. Golovach, V. I. Ochkur, V. I. Rakhovskii, N. M. Romyantsev, and V. M. Shustryakov, *Zh. Eksp. Teor. Fiz.* **93**, 65 (1987) [Sov. Phys.—JETP **66**, 36 (1987)].
- ⁴⁴D. L. Ziegler, J. H. Newman, L. N. Goeller, K. A. Smith, and R. F. Stebbings, *Planet. Space Sci.* **30**, 1269 (1982).
- ⁴⁵M. Mali, P. N. Volovich, V. L. Ovchinnikov, and L. L. Shimon, in *Abstracts of Contributed Papers, Fourteenth International Conference on the Physics of Electronic and Atomic Collisions, Palo Alto, 1985*, edited by M. J. Coggiola, D. L. Huestis, and R. P. Saxon (North-Holland, Amsterdam, 1986), p. 707.
- ⁴⁶J. C. Halle, H. H. Lo, and W. L. Fite, *Phys. Rev. A* **23**, 1708 (1981).
- ⁴⁷T. R. Hayes, R. C. Wetzel, and R. S. Freund, *Phys. Rev. A* **35**, 578 (1987).
- ⁴⁸R. J. Shul, R. C. Wetzel, and R. S. Freund, *Phys. Rev.* **39**, 5588 (1989).
- ⁴⁹T. R. Hayes, R. C. Wetzel, F. A. Baiocchi, and R. S. Freund, *J. Chem. Phys.* **88**, 823 (1988).
- ⁵⁰Colutron Research Corp., Boulder, CO 80301; L. Wahlin, *Nucl. Instrum. Methods* **27**, 55 (1964).
- ⁵¹D. H. Crandall, R. A. Phaneuf, R. A. Falk, D. S. Belić, and G. H. Dunn, *Phys. Rev. A* **25**, 143 (1982).
- ⁵²D. H. Aue, H. M. Webb, and M. T. Bowers, *J. Am. Chem. Soc.* **97**, 4136 (1975); **98**, 311 (1976).
- ⁵³C. Utsunomiya, T. Kobayashi, and S. Nagakura, *Chem. Phys. Lett.* **39**, 245 (1976).
- ⁵⁴F. A. Baiocchi, R. C. Wetzel, and R. S. Freund, *Phys. Rev. Lett.* **53**, 771 (1984).
- ⁵⁵T. R. Hayes, R. J. Shul, F. A. Baiocchi, R. C. Wetzel, and R. S. Freund, *J. Chem. Phys.* **89**, 4035 (1988).
- ⁵⁶R. J. Shul, T. R. Hayes, R. C. Wetzel, F. A. Baiocchi, and R. S. Freund, *J. Chem. Phys.* **89**, 4042 (1988).
- ⁵⁷M. F. A. Harrison, *Br. J. Appl. Phys.* **17**, 371 (1966).
- ⁵⁸F. W. Lampe, J. L. Franklin, and F. H. Field, *J. Am. Chem. Soc.* **79**, 6129 (1957).
- ⁵⁹B. A. Tozer and J. D. Craggs, *J. Electron. Control* **8**, 103 (1960).
- ⁶⁰R. K. Asundi and M. V. Kurepa, *J. Electron. Control* **15**, 41 (1963).
- ⁶¹J. A. Beran and L. Kevan, *J. Phys. Chem.* **73**, 3866 (1969).
- ⁶²A. G. Harrison, E. G. Jones, S. K. Gupta, and G. P. Nagy, *Can. J. Chem.* **44**, 1967 (1966).
- ⁶³R. Alberti, M. M. Genoni, C. Pascual, and J. Vogt, *Int. J. Mass. Spectrom. Ion Phys.* **14**, 89 (1974).
- ⁶⁴J. E. Bartmess and R. M. Georgiadis, *Vacuum* **33**, 149 (1983).
- ⁶⁵B. Cabaud, A. Hoareau, P. Nounou, and R. Uzan, *Int. J. Mass Spectrom. Ion Phys.* **8**, 181 (1972).
- ⁶⁶R. E. Walstedt and R. F. Bell, *J. Chem. Phys.* **87**, 1423 (1987).
- ⁶⁷N. C. Blais and J. B. Mann, *J. Chem. Phys.* **33**, 100 (1960).
- ⁶⁸S. M. Younger, *Phys. Rev. A* **35**, 4567 (1987).
- ⁶⁹S. M. Younger, *Phys. Rev. A* **35**, 2841 (1987).
- ⁷⁰R. Colin, P. Goldfinger, and M. Jeunehomme, in *Proceedings of the ASTM Conference on Mass Spectrometry, Chicago, 1961* (unpublished), p. 1.
- ⁷¹R. F. Pottie, *J. Chem. Phys.* **44**, 916 (1966).
- ⁷²L. T. Theard and D. L. Hildenbrand, *J. Chem. Phys.* **41**, 3416 (1964).
- ⁷³G. Verhaegen and J. Drowart, *J. Chem. Phys.* **37**, 1367 (1962).
- ⁷⁴J. L. Cooper, Jr., G. A. Pressley, Jr., and F. E. Stafford, *J. Chem. Phys.* **44**, 3946 (1965).
- ⁷⁵M. Ackerman, F. E. Stafford, and G. Verhaegen, *J. Chem. Phys.* **36**, 1560 (1962).
- ⁷⁶A. W. Searcy, W. S. Williams, and P. O. Schissel, *J. Chem. Phys.* **32**, 957 (1960).
- ⁷⁷M. Ackerman, F. E. Stafford, and J. Drowart, *J. Chem. Phys.* **33**, 1784 (1960).
- ⁷⁸E. D. Cater, E. G. Rauh, and R. J. Thorn, *J. Chem. Phys.* **35**, 619 (1961).
- ⁷⁹G. DeMaria, R. P. Burns, J. Drowart, and M. G. Inghram, *J. Chem. Phys.* **33**, 1373 (1960).
- ⁸⁰M. Ackerman, J. Drowart, F. E. Stafford, and G. Verhaegen, *J. Chem. Phys.* **36**, 1557 (1962).
- ⁸¹J. J. Thomson, *Philos. Mag.* **23**, 449 (1912).
- ⁸²M. Gryzinski, *Phys. Rev.* **138**, A336 (1965).
- ⁸³E. J. McGuire, *Phys. Rev. A* **3**, 267 (1971); **16**, 62 (1977).
- ⁸⁴J. W. Otvos and D. P. Stevenson, *J. Am. Chem. Soc.* **78**, 546 (1956).
- ⁸⁵J. B. Mann, *J. Chem. Phys.* **46**, 1646 (1967).
- ⁸⁶W. Lotz, *Z. Phys.* **232**, 101 (1970).
- ⁸⁷W. Lotz, *J. Opt. Soc. Am.* **60**, 206 (1970).